Molecular Therapy
Original Article

Sonic Hedgehog Effectively Improves Oct4-Mediated Reprogramming of Astrocytes into Neural Stem Cells

Hao Yang,[1] Cuicui Liu,[1] Hong Fan,[1] Bo Chen,[1] Dageng Huang,[2] Lingling Zhang,[1] Qian Zhang,[1] Jing An,[1] Jingjing Zhao,[1] Yi Wang,[1] and Dingjun Hao[1,2]

[1]Translational Medicine Center, Hong Hui Hospital, Xi'an Jiaotong University, Shaanxi 710054, China; [2]Department of Spine Surgery, Hong Hui Hospital, Xi'an Jiaotong University, Shaanxi 710054, China

Irreversible neuron loss following spinal cord injury (SCI) usually results in persistent neurological dysfunction. The generation of autologous neural stem cells (NSCs) holds great potential for neural replenishment therapies and drug screening in SCI. Our recent studies demonstrated that mature astrocytes from the spinal cord can directly revert back to a pluripotent state under appropriate signals. However, in previous attempts, the reprogramming of astrocytes into induced NSCs (iNSCs) was unstable, inefficient, and frequently accompanied by generation of intermediate precursors. It remained unknown how to further increase the efficiency of astrocyte reprogramming into iNSCs. Here, we show that mature astrocytes could be directly converted into iNSCs by a single transcription factor, Oct4, and that the iNSCs displayed typical neurosphere morphology, authentic NSC gene expression, self-renewal capacity, and multipotency. Strikingly, Oct4-driven reprogramming of astrocytes into iNSCs was potentiated with continuous sonic hedgehog (Shh) stimulation, as demonstrated by a sped-up reprogramming and increased conversion efficiency. Moreover, the iNSC-derived neurons possessed functionality as neurons. Importantly, crosstalk between Sox2/Shh-targeted downstream signals and phosphatidylinositol 3-kinase/cyclin-dependent kinase 2/Smad ubiquitin regulatory factor 2 (PI3K/Cdk2/Smurf2) signaling is likely involved in the mechanisms underlying this cellular event. The highly efficient reprogramming of astrocytes to generate iNSCs will provide an alternative therapeutic approach for SCI using autologous cells.

INTRODUCTION

The inevitable neuronal loss caused by traumatic injuries to the CNS and by degenerative diseases is particularly devastating and usually leads to sensorimotor function deficits.[1–3] Until now, there have been no curative treatments available for spinal cord injury (SCI), and existing therapeutic approaches, including surgical interventions and medications, are extremely erratic and carry severe side effects.[4–6] Fortunately, cell replacement or replenishment therapy through neural stem cell (NSC) transplantation is a promising approach to combat irreversible neuron loss accompanying various severe insults and ultimately achieves both structural and functional neurological recovery. However, the therapeutic application of NSCs in neural regeneration still faces formidable challenges, such as very limited cell sources, immunorejection, and inflammatory reaction.[7,8] Notwithstanding several other types of stem cells, including embryonic stem cells (ESCs), induced pluripotent stem cells (iPSCs), and mesenchymal stem cells (MSCs), also possess great potential to give rise to neurons, transplantation of such cells cannot circumvent several significant hurdles, for example, ethical controversies, tumorigenesis, and differentiation uncertainty.[9–12] Recently, great progress has been made in the development of cell reprogramming technologies, eliminating the aforementioned issues and enabling the generation of various cell types of interest.[13,14] Moreover, compelling studies have demonstrated that among the multiple types of somatic cells currently available, fibroblasts can be extensively used for cellular reprogramming into other closely related cell types, mainly owing to their easier accessibility, higher yield, and greater proliferation than other cell types. Thus, fibroblasts have been hitherto regarded as the most promising candidates for viable cell-based therapies.[15–18] Despite their great potential, lineage switching is a requisite for the generation of expandable induced NSCs (iNSCs) from fibroblasts, and artificial induction of expandable iNSCs has remained elusive. In addition, fibroblast-derived neuron-like cells usually failed to establish a functional synapse and neuronal circuitry, although they resemble authentic neurons.[19–21] Therefore, seeking a more appropriate source of readily accessible cells without undergoing a lineage switching is crucial for the development of cell-based therapies for SCI.

Astrocytes are broadly distributed and comprise nearly half of the cells in the mammalian CNS. The ubiquitous glial cells throughout the CNS play diverse and vital roles in the development and normal functioning of the CNS.[22,23] Recently, increasing research groups

Received 13 November 2018; accepted 4 May 2019;
https://doi.org/10.1016/j.ymthe.2019.05.006.

Correspondence: Hao Yang, Translational Medicine Center, Hong Hui Hospital, Xi'an Jiaotong University, Shaanxi 710054, China
E-mail: yanghao.71_99@yahoo.com
Correspondence: Dingjun Hao, Department of Spine Surgery, Hong Hui Hospital, Xi'an Jiaotong University, Shaanxi 710054, China
E-mail: haodingjun@126.com

have reported that astrocytes can regain pluripotency and even revert to an initiative undifferentiated state after, e.g., stroke, SCI, focal ischemia, and kainate-induced neuroexcitotoxicity.[21,24–26] More strikingly, numerous studies have further revealed that astrocytes can be converted into pluripotent NSCs, lineage-restricted neural progenitors, and even certain subtypes of neurons by forced expression of defined factors or by application of specific interventions.[27–32] In addition, reprogramming of astrocytes to directly generate iNSCs can be achieved without neural cell lineage switching and even any invasive grafts.[28,32] Thus, astrocytes are likely to be a more suitable endogenous source of cells for the treatment of CNS injuries and various neurological disorders. Indeed, we have previously shown that astrocytes from the spinal cord can be reprogrammed *in vitro* into NSCs capable of redifferentiating into neurons and glial cells, and the molecular mechanisms underlying astrocyte reprogramming may be intimately related to some viable molecules secreted from injured astrocytes within the CNS microenvironment.[20,21,33] However, several major obstacles must be overcome to increase the efficiency of astrocyte reprogramming and to reduce incomplete reprogramming, because reprogrammed astrocytes are partially converted into intermediate precursors.

In the present study, we present an efficient induction approach for the direct conversion of astrocytes into NSCs with a characteristic morphology and phenotype. We found that ectopic expression of Oct4 alone elicits reprogramming of astrocytes into iNSCs, which eventually differentiate into neurons and glial cells. Remarkably, Oct4-mediated direct reprogramming is further enhanced by continuously treating cells with sonic hedgehog (Shh). Using this strategy, we achieved three significant breakthroughs. First, the use of a single neural progenitor transcription factor, Oct4, as a reprogramming factor eliminated some of the risks, complexity of manipulation, and instability of epigenetic modifications associated with the use of multiple transcription factors. Second, the reprogramming efficiency could be efficiently enhanced by a defined factor Shh, thus bypassing a partial or incomplete intermediate state. Reprogrammed astrocytes that do not undergo neural cell lineage switching are likely to be more appropriate cell sources for cell-based therapies for SCI than other cell types. Of significance, Sox2/Shh-targeted downstream cascades and phosphatidylinositol 3-kinase/cyclin-dependent kinase 2/Smad ubiquitin regulatory factor 2 (PI3K/Cdk2/Smurf2) signaling pathways are involved in this intricate cellular transformation. Our strategy using a single transcription factor in combination with a defined factor facilitates future therapeutic applications for the repair of injured spinal cord via autologous cell-based replacement.

RESULTS

Characterization and Identification of Mature Astrocytes

To investigate whether synergistic Oct4 and Shh signaling potentiates the reprogramming of astrocytes into NSCs, we first cultured, characterized, and identified primary astrocytes from rat spinal cords. Phase-contrast microscopy showed that the large majority of cells exhibited a flat and polygonal morphology, and formed a confluent monolayer, in which there were some cells with small soma and short processes after 10 days *in vitro* (Figure 1A). After 5 days of purification, the purified astrocytes exhibited flat and polygonal shapes, and had reached more than 99% confluence (Figure 1B). To validate the identity of the purified cells, double immunostaining with glial fibrillary acidic protein (GFAP) and glutamate transporter 1 (GLT-1), GFAP, and S100b was subsequently carried out, respectively. These cells were positive not only for the typical astrocyte marker GFAP, but also for GLT-1 and S100b (Figures 1C–1E), indicating that these cells were terminally mature astrocytes. Notably, nestin reactivity was undetectable in GFAP-positive cells (Figure 1F), excluding contamination with neural precursor cells or intermediate progenitors. In agreement with the immunostaining observations, quantitative studies revealed that GFAP-positive cells maintained a high percentage (over 97% purity) in cultures, even after undergoing consecutive subculture for at least five passages (Figure 1G). In addition, quantitative real-time PCR demonstrated less characteristic gene expression, including that of nestin, Oligo2, CD133, Pax6, and A2B5 in the cells (Figure 1H), further demonstrating that there were few NSCs or neural intermediate progenitors in our cultures.

Identification of the Oct4-pGMLV Lentiviral Vector and Transduction of Astrocytes

To further confirm our hypothesis, the lentiviral vector Oct4-pGMLV was first constructed, packaged, sequenced, and used to infect astrocytes. To verify that the vector was constructed correctly, restriction endonuclease digestion, specific PCR, and agarose gel electrophoresis were performed using isolated primers. As shown in Figure S1, the Oct4 fragment was obtained from four positive clones. Notably, Oct4 was undetectable in the mock vector, suggesting that the vector encoding Oct4 was constructed correctly in our experiment (Figure S1A). Furthermore, Oct4 lentiviral particles were generated by transfection of 293T cells. After 12–36 h of transfection, Oct4 expression in 293T cells was clearly detected. Similar results regarding Oct4 expression were obtained by means of western blotting methods. Of note, the highest expression of Oct4 was observed at 36 h (Figure S1B). Double immunostaining also revealed that Oct4 expression was present in astrocytes infected with Oct4 lentiviral particles. In contrast, Oct4 expression was undetectable in the control or mock groups (Figures S1C–S1F).

Generation of NSCs from Rat Astrocytes

To visualize the conversion process from astrocytes into NSCs, we infected rat astrocytes with lentivirus encoding Oct4 in the presence of Shh and observed their morphological changes. For more clarification of the reprogramming of astrocytes to NSCs, an experimental outline is shown in Figure 2A. Next, we assessed morphology and biochemical phenotype of the reprogramming cells. As shown in Figure 2B, Oct4 transduction clearly changed astrocytes from a flat, polygonal morphology to a round morphology and even resulted in the generation of multiple cell clusters with varying sizes. Remarkably, over 3 days after Oct4 transduction, increasing cell clusters with distinct sizes, closely resembling neurospheres, had emerged and gradually expanded with longer culture. Beyond 10 days post-infection, the majority of aggregates had completely detached and become free-floating neurospheres, whereas the mock-infected or control astrocytes

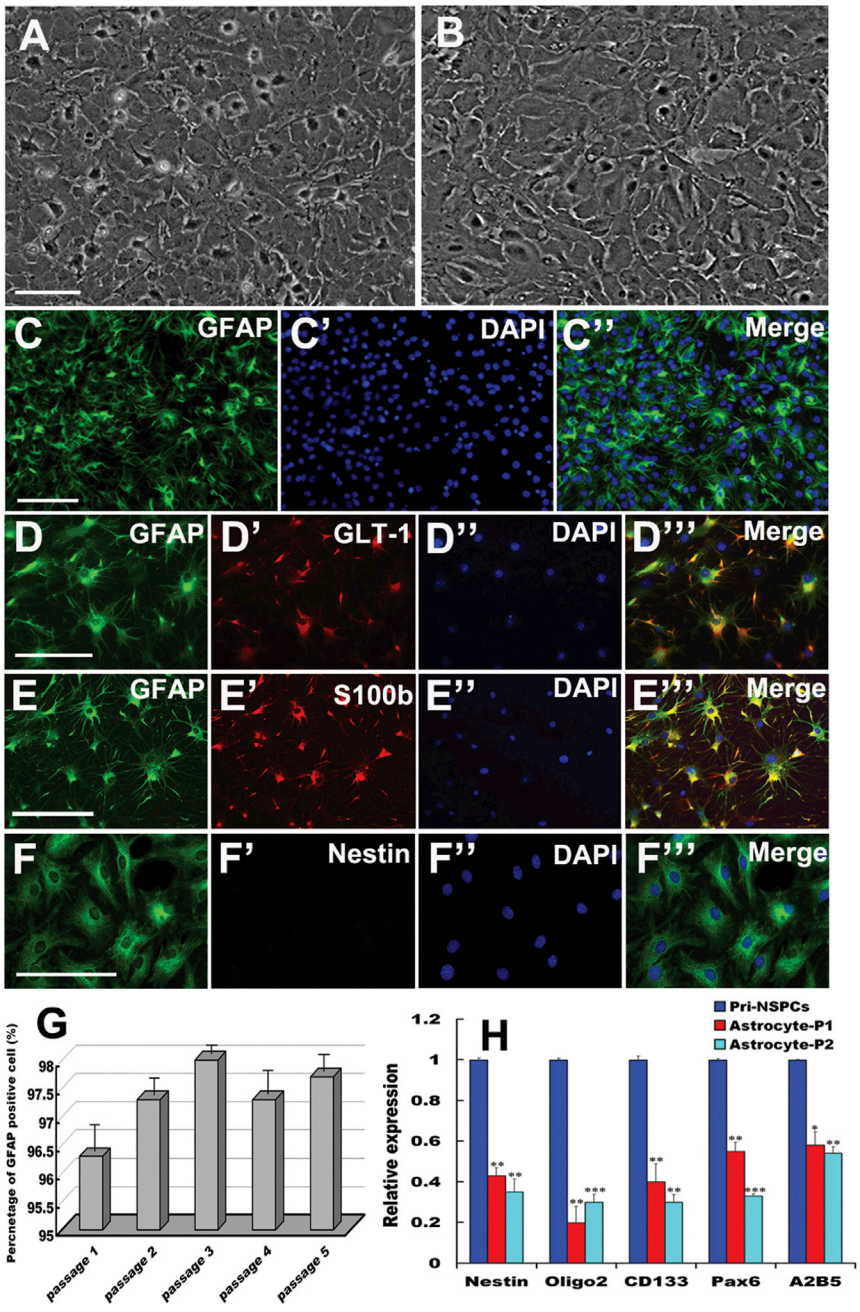

Figure 1. Morphological and Biochemical Characteristics of Primary Astrocytes

(A) Primary astrocytes at 10 days *in vitro*. (B) Astrocytes after purification at 5 days *in vitro*. (C–C′′ Representative photomicrographs of immunofluorescence for GFAP. (D–D′′′ and E–E′′′) Double immunostaining with GFAP and glutamate transporter 1 (GLT-1), GFAP, and S100b in purified cells, respectively. (F–F′′′) Immunostaining of GFAP and nestin in cells. (C′, D′′, E′′, and F′′) Notably, these panels represent DAPI staining. (G) Percentages of GFAP-immunoreactive cells among purified cells after sub-culture from passages 1–5. (H) Expression of NSC and/or neural intermediate precursor markers in purified astrocytes as analyzed by quantitative real-time PCR. Gene expression was normalized to that in primary NSCs (pri-NSCs). The error bars indicate the SD of triplicate values. All data are reported as the means ± SEM. *$p < 0.05$, **$p < 0.01$, and ***$p < 0.001$ compared with the relevant controls. Scale bars, 100 μm.

showed minimal morphological changes and generated hardly any neurosphere-like colonies during the whole process. Strikingly, when Shh was added to astrocyte cultures infected with Oct4 virus, the reprogramming efficiency was further potentiated at the same time points; the cells displayed dramatic morphological transition, formed more neurospheres, and showed higher proliferation than those with only Oct4 transduction, suggesting that Shh and Oct4 synergistically improved the reprogramming of astrocytes. To test whether the neurospheres derived from these astrocytes were NSCs, we monitored nestin expression during the reprogramming process at days 10–15 post-infection and compared it with that of the converted cells. Our results revealed that these neurospheres can incrementally express nestin during reprogramming. The number and size of nestin-positive neurospheres from astrocytes transduced with Oct4 in combination with Shh stimulation were significantly higher and larger than those from astrocytes transduced only with Oct4 (Figure 2C). Consistent with the morphological observations, quantitative analysis revealed that after Oct4 transduction, the number of neurospheres gradually increased with prolongation of time, whereas the addition of Shh to the culture resulted in significant 1.2- to 2.5-fold increases in the number of neurospheres over the four indicated durations (Figure 2D).

Oct4 Directs Astrocytes to Acquire Biochemical Phenotypic Characteristics of NSCs

To systematically validate whether the combination of Oct4 transduction and Shh stimulation (Oct4/Shh) effectively strengthens astrocyte reprogramming, we further investigated a subset of characteristic molecules for NSCs and astrocytes at the mRNA and protein levels, and subsequently profiled the transcriptome. As shown in Figures 3A–3C, within 15 days of Oct4/Shh treatment, RT-PCR analyses indicated that several selected NSC markers, nestin, Pax6, and CD133, were gradually increased at the mRNA levels in cells, whereas the astrocyte-specific marker GFAP was drastically downregulated. In contrast, the combination of Oct4/Shh significantly changed the protein levels of the aforementioned molecules, as demonstrated by a marked change in band densitometry. Similar to the RT-PCR

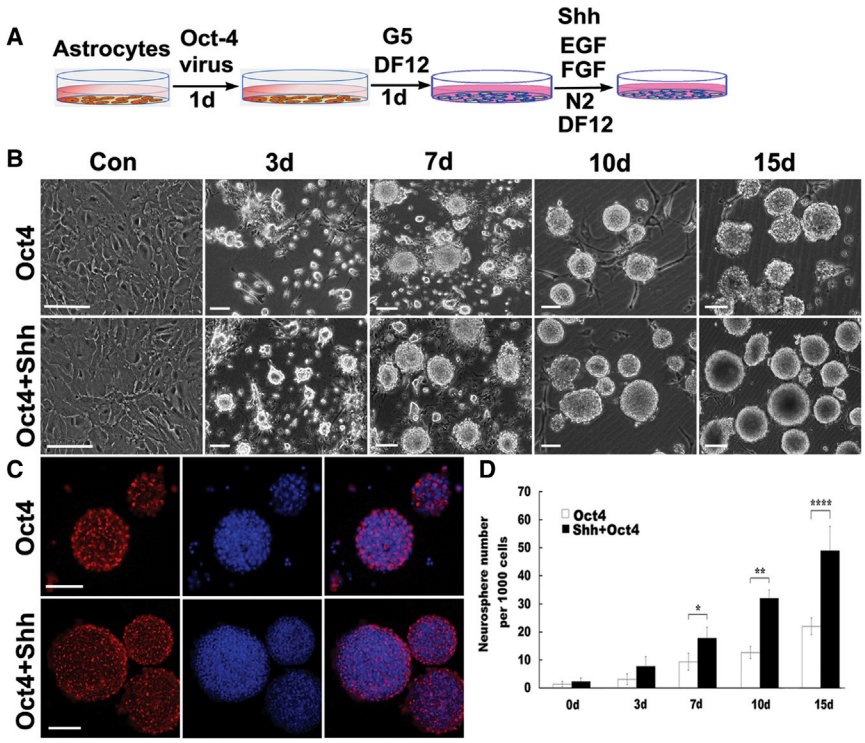

Figure 2. Generation and Characterization of iNSCs from Rat Astrocytes

(A) Schematic illustration depicting the procedure for the reprogramming of astrocytes into NSCs. (B) Phase-contrast images of astrocytes transfected with Oct4 lentivirus with or without Shh stimulation at the indicated times. Notably, astrocytes cultured in NSC medium without Oct4 lentivirus transduction and mock-transduced astrocytes did not generate neurospheres or clusters (see the upper left panels). (C) Expression of nestin in neurospheres at 10–15 days following Oct4 virus infection in the presence or absence of Shh as revealed by immunostaining. (D) Quantitative analysis of neurosphere generation at the indicated time points after treatment with Oct4 or Oct4/Shh. There were significantly more neurospheres in Oct4/Shh-induced samples at the indicated time points. The data are presented as the mean ± SEM of three independent experiments. *$p < 0.05$ indicated a significant difference compared with the corresponding controls; **$p < 0.01$; ****$p < 0.0001$. Scale bars, 150 μm.

analyses, quantitative real-time PCR analysis demonstrated that the levels of the transcript expression of nestin, Pax6, and CD133 transcripts presented a gradually elevated tendency in astrocytes after Oct4 transduction, whereas GFAP showed a declining trend. In contrast, delayed addition of Shh to Oct4-transduced cells further improved reprogramming efficiency, inducing higher expression levels of the NSC markers. Interestingly, as a result of a change in cell fate, the expression of the astrocyte marker gene GFAP was drastically reduced (Figure 3B). In comparison, the change tendency is more dramatic in Oct4/Shh-treated astrocytes than that of Oct alone. In agreement with the results for the gene transcripts, western blotting revealed that the expression of aforementioned NSC markers exhibited a similar tendency from 3 to 15 days post-Oct4 transduction. Likewise, the delivery of Shh to the culture dramatically elevated the expression levels of the NSC markers. Regarding GFAP expression, a significant decrease was found after Oct4 transduction in the presence or absence of Shh (Figure 3C). In line with this, quantification analysis revealed that the reprogramming of astrocytes was effectively enhanced by Oct4 transduction in the presence of Shh (Figure 3D).

To further confirm the validity of the reprogramming protocol, we profiled the transcriptomes of astrocytes, Oct4-induced astrocytes, Oct4/Shh-induced astrocytes, and primary NSCs (pri-NSCs) (wild-type) by RNA sequencing (RNA-seq), and analyzed the similarities between them. Heatmap with hierarchical cluster analysis, Vena, and scatterplots of gene expression levels among Oct4-induced astrocytes (5 and 7 days post-Oct4 transduction), Oct4/Shh-induced astrocytes (5 and 7 days post-Oct4 transduction in combination with Shh), and pri-NSCs revealed that numerous genes were upregulated or downregulated in expression levels in the induced NSCs and NSCs, and that pri-NSCs were highly distinguished from astrocytes but were similar to Oct4-induced or Oct4/Shh-iNSC-like cells (Figures 3E–3G; Figures S2–S7). Notably, the similarity between pri-NSCs and Oct4-induced astrocytes at 5 and 7 days was gradually elevated with time. As for the Oct4/Shh-iNSC-like cells, the global gene expression pattern was more similar to that of pri-NSCs than to that of Oct4-induced cells. In addition, the expression of numerous genes in Oct4/Shh-iNSC-like cells showed higher similarity to that in pri-NSCs than at 5 days (Figures 3F and 3G). Gene Ontology (GO) enrichment analysis of the upregulated genes that are relevant to neurogenesis, nerve development, mitotic cell cycle, cell division, and axonal extension between NSCs astrocyte-derived NSCs (induced with Oct4 and Shh or not) and astrocytes showed that the astrocyte-derived NSCs are similar to that of NSCs in the capacity to proliferate and self-renew, albeit somewhat distinct (Figures S4 and S5). Further test by quantitative real-time PCR assay confirmed that a series of representative genes selected from NSCs and many genes relevant to fate-determinant, self-renewal, and stemness were significantly upregulated (Figure 3H).

Self-Renewal Capacity of NSC-like Cells Reprogrammed from Astrocytes

In addition to the acquisition of NSC morphology and biochemical phenotypic characteristics associated with NSCs, self-renewal potential is also a crucial hallmark of NSCs. Thus, cell proliferation was assessed and quantitated using bromodeoxyuridine (BrdU) incorporation assays and flow cytometric analysis. At 3 and 7 days after the above-mentioned treatments, the number of $BrdU^+$ cells in the Oct4/Shh induction group was significantly higher than that in

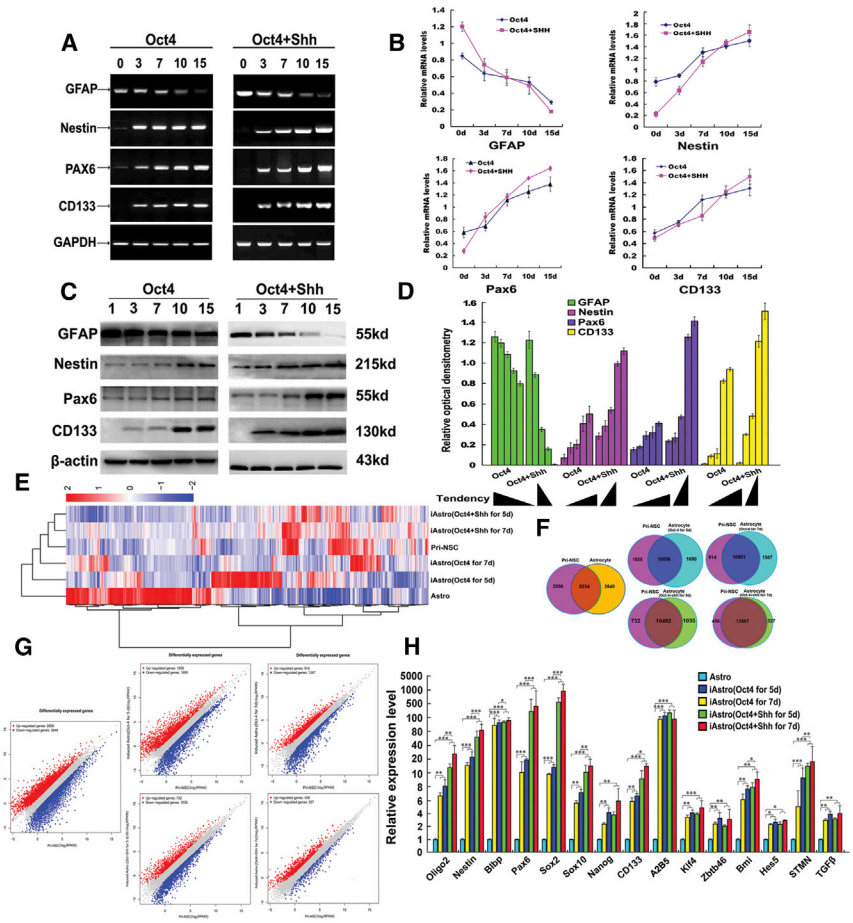

Figure 3. Phenotypic Characteristics and Transcriptome Profiling of Oct4-Transduced Astrocytes in the Presence of Shh

(A) Gene expression characteristics of astrocytes under different treatment conditions as assessed by RT-PCR at the indicated time points. Representative RT-PCR products for each marker are shown. NSC markers, such as nestin, Pax6, and CD133, were upregulated, whereas the astrocyte marker GFAP was dramatically downregulated or even absent. (B) qPCR results showing the mRNA levels of the aforementioned genes under the indicated treatments at the indicated time points. (C) Western blots revealing the expression of the NSC antigens nestin, Pax6, and CD133 in astrocyte cultured under the two indicated conditions at the above-mentioned time points. (D) Quantification of relative expression of the above-mentioned intensity of immunoblots. β-Actin served as a loading control of total proteins. (E) Heatmap representing the global expression profile of astrocytes, induced astrocytes (Oct4/Shh and Oct4 at 5 and 7 days), and pri-NSCs are classified into the same hierarchical cluster. (F) Venn diagram of differentially expressed genes shared between reprogrammed astrocytes and NSC or astrocytes. The differential genes are indicated. (G) Pairwise scatterplot analysis of the global expression profiles of astrocytes, pri-NSCs, and induced astrocytes (Oct4 or Oct4/Shh at 5 and 7 days). The transcriptome of each cell type was profiled by RNA-seq analysis. Relative gene expression levels (RPKM) are depicted in $\log_{10}$ scale. (H) Quantitative real-time PCR analyses of selected genes in NSCs and some genes involved in cell fate-determinant, self-renewal, and stemness from differentially induced astrocytes. Gene expression was normalized to that in astrocytes. *$p < 0.05$; **$p < 0.01$; ***$p < 0.001$ compared with their respective controls.

the Oct4 transduction group or the control group (Figure 4A). Quantification analysis revealed that there was a significant difference in the percentage of $BrdU^+$ astrocytes among the three groups (3 days after treatment: 6.61% ± 0.58% for control, 12.9% ± 3.28% for Oct4 transduction alone, 23.9% ± 2.83% for Oct4/Shh-induction; 7 days after treatment: 3.89% ± 0.87% for control, 21.6% ± 3.16% for Oct4 transduction alone, 29.8% ± 3.43% for Oct4/Shh-induction) (Figure 4B) ($p < 0.01$ and $p < 0.001$ versus the corresponding controls), and the corresponding percentage of proliferative cells at 7 days was higher than that at 3 days, suggesting that Oct4/Shh co-stimulation enhances the proliferative ability of reprogrammed astrocytes. To further substantiate this claim, flow cytometric analysis was used to evaluate cell proliferation by assessing cell-cycle distribution. The flow cytometry data showed cell-cycle changes in the astrocytes 3 and 7 days after the indicated treatments (Figure 4C). Similar to the findings of BrdU staining, at 3 and 7 days after Oct4/Shh or Shh treatment, the proportions of reprogrammed astrocytes in the G2/M phase and the S phase were remarkably raised, whereas the proportion of reprogrammed astrocytes in the G1 phase was reduced. There was a significant difference in cell-cycle distribution between reprogrammed and normal astrocytes. Notably, the percentage of reprogrammed astrocytes in the G2/M phase was significantly higher in the group receiving the combination of Oct4 and Shh than in the group receiving Oct4 alone ($p < 0.01$, $p < 0.001$) (Figure 4D). Collectively, these data suggest that the combination of Oct4 and Shh can efficiently promote the transition from G1 to S phase and G2/M phase, which represents cell re-entry into the cell cycle and gain of self-renewal capacity.

Tripotency of NSCs Reprogrammed from Astrocytes

To characterize the differentiation potential of NSCs reprogrammed from astrocytes by Oct4 transduction and Shh stimulation, the NSCs were cultured under a special differentiation condition, as is typically done for NSCs, and were further identified by immunostaining assay. As shown in Figure 5, during the 10 days after induction, the reprogrammed astrocytes gave rise to Tuj-1^+ neurons, $GFAP^+$ astrocytes, and CNP^+ oligodendrocytes over five passages. By comparison, oligodendroglial differentiation was relatively rare. Strikingly, this differentiation potential was well maintained during prolonged culture (over five passages). From the differentiated cell morphology, it seemed that NSCs reprogrammed from astrocytes by Oct4/Shh treatment differentiated more MAP2 neurons than those from astrocytes

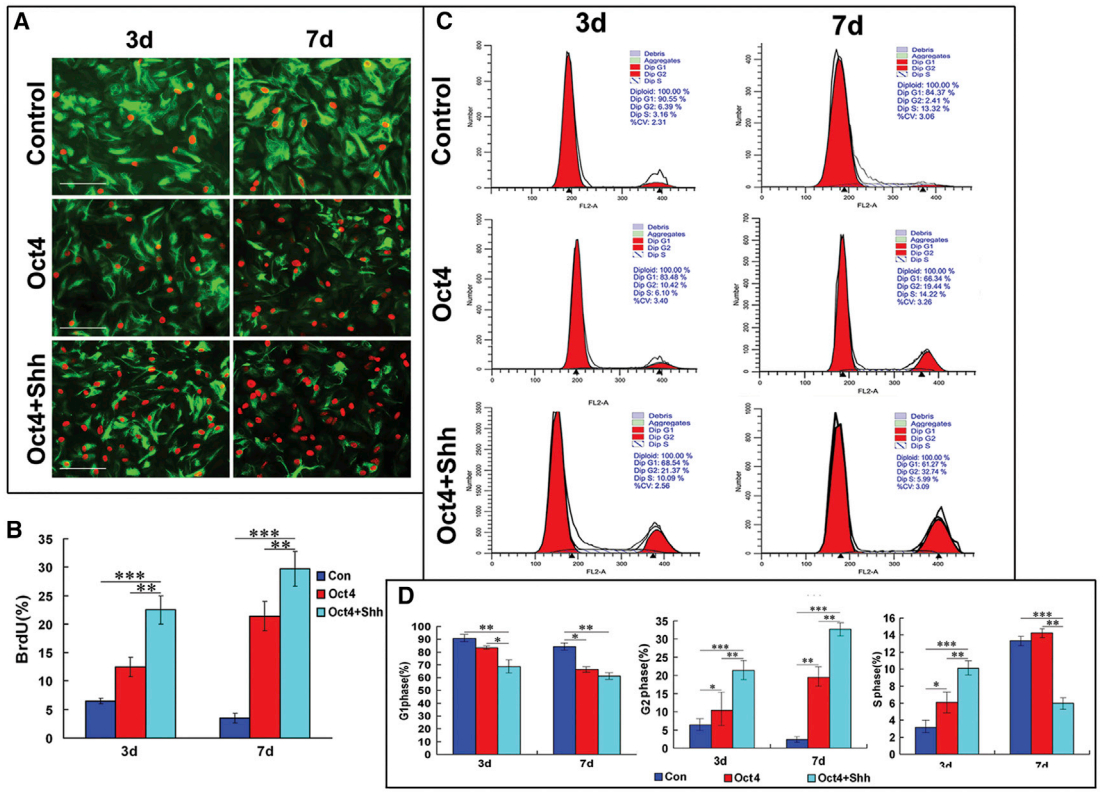

Figure 4. *In Vitro* Self-Renewal Capacity of NSC-like Cells

(A) Photomicrographs of BrdU incorporation into astrocytes transduced with Oct4 in combination with Shh stimulation, which was analyzed to assess the proliferation of NSC-like cells derived from astrocytes at 3 and 7 days. There were significantly more BrdU$^+$ cells in Oct4/Shh-induced samples at the indicated time points than in Oct4-induced and control samples. Notably, GFAP expression was also drastically decreased in Oct4/Shh-induced samples. (B) Quantification of BrdU-positive cells among cells subjected to the indicated treatments. All data are reported as the means ± SEM and are representative of three independent experiments with similar findings. $^{**}p < 0.01$ and $^{***}p < 0.001$ versus the corresponding controls. (C) Astrocytes treated under the indicated conditions for 3 and 7 days were analyzed by flow cytometry. G0/G1, G2/M, and S represent different cell phases, and the corresponding data are shown in each panel. (D) Statistical analysis of the percentages of cells in the three phases showed a significant difference between the Oct4/Shh group and the other treatments. The percentage of cell in each phase was calculated by using the cell ModiFIT program. All data are reported as the means ± SEM. $^{*}p < 0.05$, $^{**}p < 0.01$, and $^{***}p < 0.001$ versus the relevant controls. Scale bars, 100 μm.

receiving Oct4 alone (Figure 5A). Upon further differentiation, mature neurons that expressed a typical neuronal marker, MAP2, and neuronal subtypical markers, including GABA and vGuT1, were readily detected over 10 days by double immunostaining (Figure 5A, right panels), indicating generation of excitatory and inhibitory subtypes of neurons. Subsequent analysis revealed a significant difference in the percentage of Tuj-1$^+$ and GFAP$^+$ cells among the indicated treatment groups ($p < 0.05$ versus the corresponding controls), indicating that forced expression of Oct4 in combination with Shh induction greatly enhances reprogramming of astrocytes toward genuine NSCs (Figure 5B). Consistent with the immunocytochemistry results, western blot analysis also revealed similar expression patterns of GFAP, Tuj-1, MAP2, GABA, vGuT1, NeuN, and CNP (Figure 5C). To determine astrocyte-derived NSC differentiation potential *in vivo*, they were microinjected into the spinal cord of 2-month-old rats (n = 4), and their survival and differentiation were evaluated 2–3 weeks after transplantation. Strikingly, 5-chloromethylfuorescein diacetate (CFMDA)-marked astrocyte-derived NSCs could survive and efficiently differentiated MAP2-positive neurons with branching neurites, displaying double staining (Figure 5D), whereas in CFMDA-marked astrocyte injection, apart from cell migration and survival, no double staining for MAP2 and CFMDA was detectable (Figure 5E).

Astrocyte-Derived Cells Exhibited Typical Neuronal Functional Characteristics

Although converted astrocytes could give rise to neuron-like cells with wild-type neuron morphological features and gene phenotypic characteristics, it remained unknown whether these differentiated neurons were functional. Therefore, we first evaluated the expression of synapsin, a specific marker of functional neurons, by immunostaining and western blot. As shown in Figure 6A, immunostaining indicated that MAP2-positive cells were also strongly synapsin immunoreactive, displaying punctate distribution in the somatic

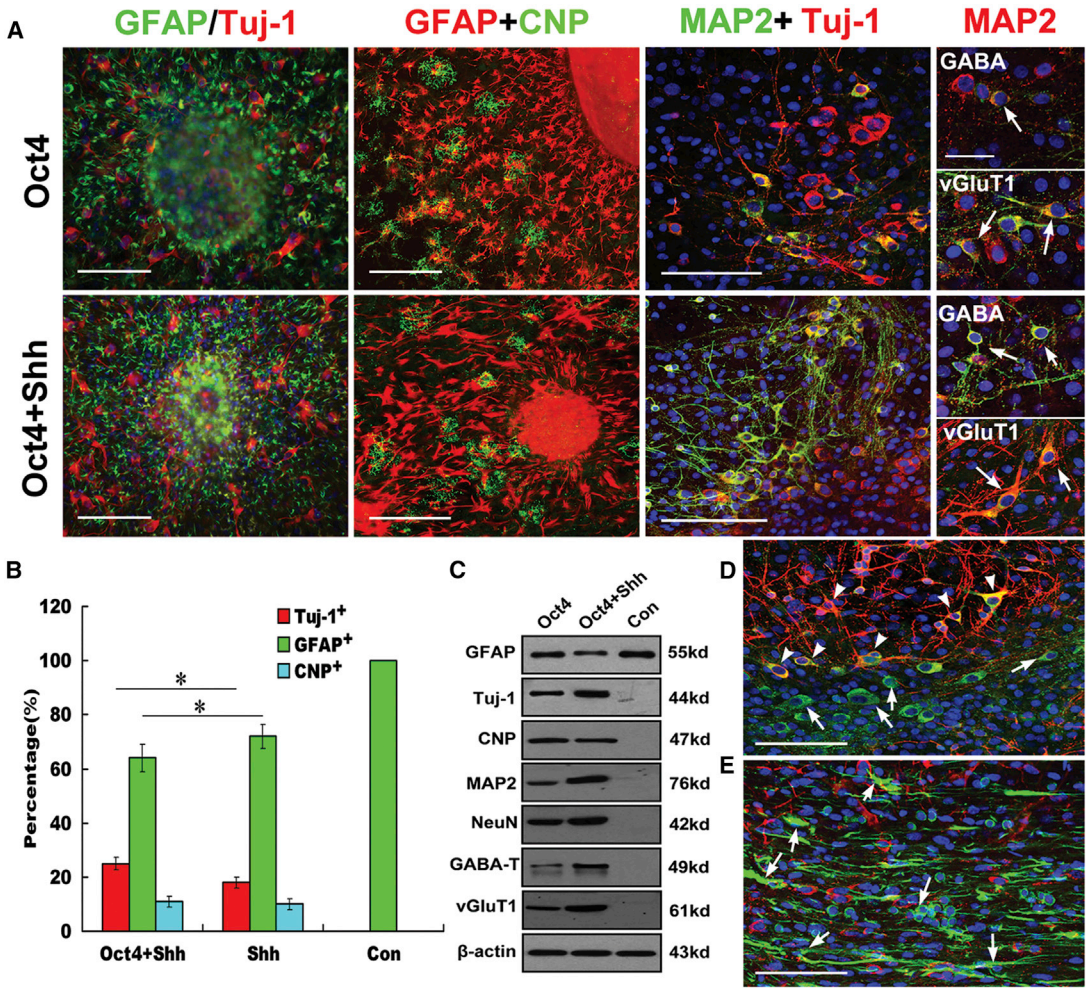

Figure 5. *In Vitro* and *In Vivo* Tripotency of iNSCs Reprogrammed from Astrocytes

(A) Immunostaining analysis showing that after a 10-day induction, neurospheres derived from astrocytes could differentiate into neurons, astrocytes, and oligodendrocytes. The overlaid images show Tuj-1$^+$ (red, arrows) neurons, GFAP$^+$ (green) astrocytes, Glc$^+$ (green) oligodendrocytes, and DAPI-stained (blue) nuclei. Determination of cell maturity of differentiated neurons by double immunostaining with MAP2 and Tuj-1, MAP2, and the indicated markers (GABA and vGluT1), respectively (right panels, arrows; scale bars, 50 μm). For normal astrocytes and those treated with Shh alone, no data are shown for no neurosphere formation. Scale bars, 150 μm. (B) Quantification of cell differentiation in neurospheres from the indicated treatment groups. The data represent the percentage of cells immunostained for neuron (Tuj-1$^+$), astrocyte (GFAP$^+$), and oligodendrocyte (CNP$^+$) markers out of the total number of cells in culture (mean ± SEM). $p < 0.05$ was used as the criterion for statistical significance. Notably, the total cell number was determined by staining with DAPI. (C) Western blot analysis of the indicated marker expression in differentiated NSCs derived from astrocytes under the indicated conditions. β-Actin served as a loading control. Notably, the expression of Tuj-1, MAP2, NeuN, GABA-T, and vGluT1 was higher in differentiated iNSCs derived from astrocytes treated with Oct4/Shh than in those derived from astrocytes or from astrocytes treated with Oct4 alone and control. (D) *In vivo* neuronal differentiation of microinjected astrocyte-derived iNSCs into spinal cord and analysis at 3 weeks after transplantation (green, CMFDA labeling; red, MAP2). (E) Astrocytes keep their glial identity without doubling staining of CMFDA and MAP2 at 3 weeks after transplantation into the spinal cord. (D and E) Arrowheads, CMFDA-labeled MAP2$^+$ cells; arrows, CMFDA-labeled cells. Scale bars, 150 μm.

membrane and neurites (see high magnifications in right panels). In the controls, no synapsin immunoreactivity was detectable (data not shown). Strikingly, synapsin showed more intense reactivity in the differentiated neurons derived from astrocytes reprogrammed with Oct4 and Shh than in those receiving Oct4 alone. Consistent with the above immunostaining results, the western blots revealed a markedly higher increase for synapsin, PSD-95, and Homer1 expression in reprogrammed cells than control cells, and higher expression of the above-mentioned markers in cells treated with Oct4 and Shh than in cells treated with Shh alone (Figure 6B).

To more rigorously characterize these differentiated neurons, we also assessed the calcium imaging properties of the iNSCs (reprogrammed astrocytes at 7 and 10 days post-Oct4 transduction with or without

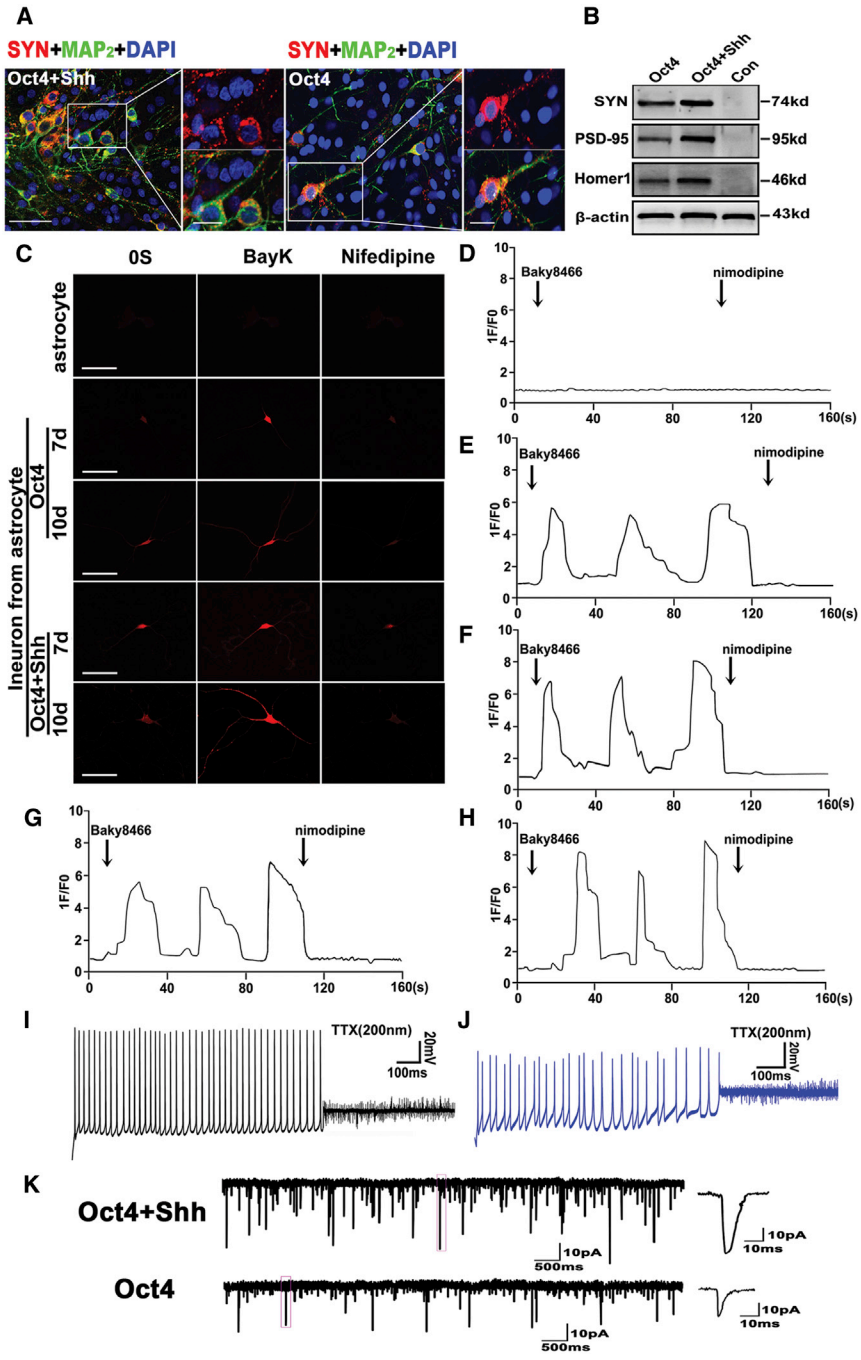

Figure 6. Functional Assays of Neurons Reprogrammed from Astrocytes

(A) Representative micrographs illustrating immunolocalization of synapsin in iNSC-derived neurons at 15 days post-induction. Scale bars, 50 μm; 15 μm (high-magnification panel). (B) Western blot analysis of synapsin PSD-95 and Homer1 expression in iNSC-derived cells at 15 days post-induction. β-Actin served as a loading control for the total proteins. (C) Representative calcium images for astrocytes or differentiated neurons derived from iNSCs. The panels show typical calcium images observed in neurons derived from 7-day and 10-day reprogrammed astrocytes (iNSCs) after 15 days of differentiation. Scale bars, 150 μm. (D–H) Functional characteristics of the L-type calcium channel. Changes in the calcium response in astrocytes or differentiated neurons (D, astrocytes; E and F, differentiated neurons derived from 7-day and 10-day iNSCs treated with Oct4 alone, respectively; G and H, differentiated neurons derived from 7-day and 10-day iNSCs treated with Oct4/Shh, respectively) with or without nifedipine after treatment with BayK. 1F/F0 represents the ratio of the cell fluorescence intensity at the indicated time to the fluorescence intensity at 0 s. BayK (10 mM) in the presence or absence of nifedipine (5 mM) was administered at the indicated time points. The total number of cells tested in each experiment was approximately 50; representative results are presented. (I) iNSC-derived neurons (induced by a combination of Oct4 and Shh induction) generated spontaneous action potentials with a native neuron firing pattern including regular spiking with the same amplitude. (J) iNSC-derived neurons (induced by Oct4 alone) fired irregular and instable spontaneous action potentials with unequal amplitudes. (K) Representative spontaneous postsynaptic currents (sPSCs) in iNSC-derived neurons. Notably, the iNSC-derived neurons (induced with Oct4/Shh) exhibited larger amplitudes and higher frequencies.

Shh induction) following 3 weeks of differentiation. As shown in Figures 6C and 6E–6H, the induced neurons displayed increased neuron-specific calcium influx when treated with BayK, a calcium channel agonist, as indicated by an approximately 6- to 9-fold increase in fluorescence intensity at 3 weeks post-induction. After withdrawal of BayK, the converted cells continued to display elevated fluorescence intensity, which could be blocked by nifedipine, a specific L-type calcium channel blocker. Intriguingly, the addition of KCl resulted in a bit of recovery in calcium fluorescence intensity compared with the blockage of nifedipine (Figures S7A, S7C, and S7D), indicating that these differentiated neurons have acquired the physiological activity profiles of authentic neurons. In control astrocytes, no change in fluorescence intensity was observed albeit the addition of BayK to the culture medium (Figures 6A and 6D; Figures S7A and S7B). In contrast, the differentiated neurons from iNSCs induced by Oct4/Shh (Figures 6C, 6G, and 6H; Figures S7A and S7D) exhibited stronger fluorescence intensity than those from iNSCs induced by Oct4 alone (Figures 6E and 6F; Figures S7A and S7C). In addition, the fluorescence intensity was intimately associated with Oct4 transduction time (Figures 6C and 6E–6H).

Next, we examined the membrane electrophysiological properties after 3 weeks of differentiation. As shown in Figures 6I and 6J, in

current-clamp experiments, some cells (four of seven) were able to fire repetitive action potentials. In addition, the inactivating inward currents were observed that could be blocked by tetrodotoxin (TTX), a specific inhibitor of sodium ion channels, demonstrating that iNSCs could generate functional neurons *in vitro*. Notably, neurons derived from astrocytes reprogrammed by combining with Oct4 and Shh fired regular spiking with the same amplitude, indicative of a more mature neuron firing pattern, whereas an irregular spontaneous action potential was elicited in neurons derived from astrocytes reprogrammed by Oct4 alone. In addition, the spike amplitude in the Oct4 group was significantly lower than that in the Oct4/Shh combination group, and the potential in the Oct4-only group was not stable, exhibiting various amplitudes and frequencies. Patch-clamp recording revealed significant sodium and potassium currents in induced astrocyte-derived neurons. In comparison, the currents in neurons derived from induced astrocytes with Oct4/Shh (I_{Na} = 2.17 ± 242 pA; I_k = 2.86 ± 282 pA; n = 10) were larger than that with Oct4 (I_{Na} = 1.39 ± 136 pA; I_k = 1.86 ± 182 pA; n = 10) (Figures S7E and S7F). More importantly, the derived astrocytes neurons exhibited spontaneous postsynaptic currents (sPSCs), suggesting neuron functional maturity. Notably, the neurons derived from astrocytes reprogrammed by Oct4/Shh (3 out of 10) exhibited larger amplitudes and higher frequencies than that of the neurons reprogrammed by Oct4 alone (2 out of 11) (Figure 6K).

Activation of Endogenous Neural Transcription Factors or Regulators during Astrocyte Reprogramming

To understand the molecular mechanisms of Oct4/Shh-mediated astrocyte reprogramming, we first investigated gene profile changes by using qRT-PCR assays. At day 10 after Oct4 transduction in combination with Shh stimulation, we found dramatic increases, up to 62,000-fold, 960-fold, and 85-fold, respectively, in the transcript levels of two critical transcription factors, Oct4 and Sox2, and NSC marker nestin. In contrast, Oct4 transduction alone resulted in 3,100-fold, 65-fold, and 25-fold increases, in Oct4, Sox2, and nestin, respectively, suggesting that Oct4 enhanced the reprogramming of astrocytes into NSCs, but that the addition of Shh greatly strengthened the reprogramming efficiency (Figure 7A). Next, we performed immunostaining of Sox2 to examine the critical transcription factor expression changes during the reprogramming process. Interestingly, we found more Sox2-positive cells with intense immunoreactivity for Sox2 among astrocytes treated with Oct4/Shh than among astrocytes transduced only with Oct4 (Figure 7B). As for astrocytes treated with Shh alone, no Sox2-positive cells were found (data not shown). To further elucidate the possible molecular mechanisms underlying the enhancement of astrocyte reprogramming by Shh, several important molecules involved in the intracellular signaling cascade critical for reprogramming process were examined. As expected, quantitative real-time PCR validated that there was significant upregulation of Ptch (patched homolog), GLI family zinc-finger 2 (Gli2), and CyclinD1 expression in astrocytes treated with both Oct4 and Shh compared with control, mock-transduced, and Oct4-transduced astrocytes (Figure 7C). Similar to quantitative real-time PCR analysis, western blot analysis also showed that the expression of the aforementioned molecules was markedly elevated in astrocytes treated with Oct4/Shh. Although Oct4 alone also elicited upregulation of the three molecules in converted astrocytes, their levels were considerably lower than those in the group treated with Oct4/Shh (Figure 7C, lower right panel). Strikingly, western blot analysis further showed that the PI3K/Cdk2 signaling pathway was activated during the reprogramming of astrocytes into NSCs. More importantly, the downstream effector Nolz1, which is responsible for cell-cycle exit, was dramatically reduced in Oct4-transduced astrocytes treated with or without Shh, compared with control and mock astrocytes. Furthermore, Smurf2, a ubiquitin ligase that regulates TGFβ/Smad signaling, was significantly elevated. There was a significant difference in the expression levels of these molecules between Oct4-transduced astrocytes treated with and those not treated with Shh (Figure 7D).

Although the above-mentioned data have demonstrated that the PI3K/Cdk2 signaling cascade could be involved in this complicated event because their levels were significantly elevated in the reprogramming procedure, it is unclear whether the reprogramming of astrocyte to NSCs was inhibited when blocking them by their corresponding antagonist. Therefore, we further measured the expression levels of NSC-specific markers in astrocytes transduced with Oct4 in the presence of Shh by western blot assays. Intriguingly, with GDC-0941, SU9516, and USF2 in different combinations, the efficiency of astrocytes reprogramming was dramatically reduced as demonstrated by a 5-fold to over 10-fold decrease in the expression of nestin, Pax6, and Sox2, and even complete suppression of their expression. As for GFAP, no remarkable change was detectable but for the absence of the above-mentioned three inhibitors (Figure 7E), suggesting different contributions of PI3K/Cdk2/Smurf2 signaling, and that is likely involved in the mechanisms underlying this reprogramming event.

DISCUSSION

Neural stem cell (NSC) therapies have emerged as a promising option for treating neural injuries and neurodegeneration. Nevertheless, the difficulty in obtaining a sufficient number of pri-NSCs poses a major bottleneck in the development of successful strategies for therapeutic application. Therefore, developing an alternative strategy for generating desired cell types is crucial. Fortunately, cell reprogramming technology represents a promising avenue in cell replacement therapies owing to its potential to circumvent restriction.

In this study, we present *in vitro* data emphasizing the potential efficacy of a combination of Oct4 transduction and Shh stimulation, which efficiently enabled conversion of rat astrocytes into NSCs. The generated NSCs resemble pri-NSCs in several key aspects; for example, they have similar morphological attributes (expandable neurospheres), similar molecular phenotypic profiles, and the ability to self-renew and redifferentiate into functional neurons, astrocytes, and oligodendrocytes. Our in-depth functional studies demonstrating synapse formation, neuronal-specific Ca^{2+} imaging, sPSCs, I_{Na} and I_k, and action potential spikes from the iNSC-derived mature neurons further authenticate the effectiveness of the reprogramming method.

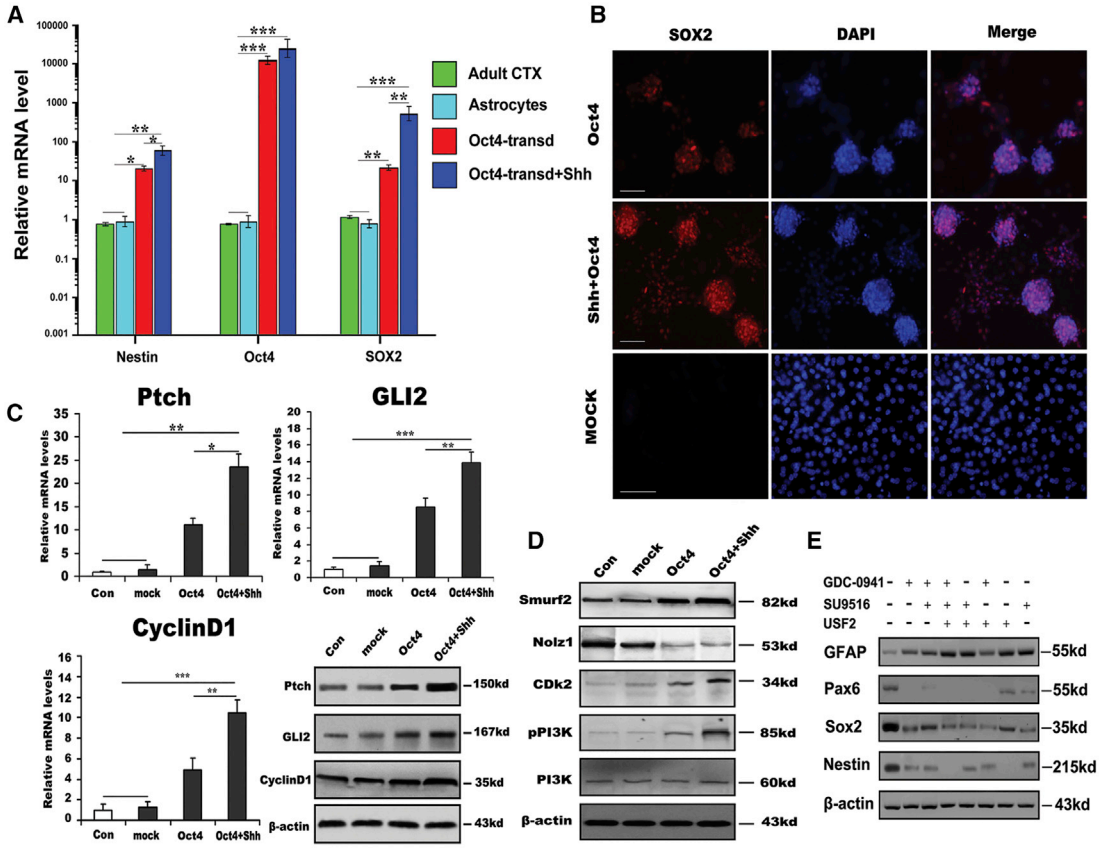

Figure 7. Possible Molecular Regulation Involved in Astrocyte Reprogramming

(A) Expression of the indicated genes in astrocyte-derived NSCs at passage 2 analyzed by quantitative real-time PCR (in three independent neurospheres from reprogrammed astrocytes). (B) Immunostaining analysis showing SOX2 expression in iNSCs (passage 2) derived from astrocytes induced by the indicated conditions depicting the enhancing effect of Shh on NSC generation and characteristics. Scale bars, 150 μm. (C) Quantitative real-time PCR and western blot analysis of Ptch, GLI2, and CyclinD1 mRNA and protein levels in astrocytes induced by the indicated conditions. (D) Western blot analysis of Smurf2, Nolz1, CDk2, PI3K, and phosphorylated PI3K expression in astrocytes under the indicated conditions after 10 days. (E) The analyses of astrocyte reprogramming mediated by Oct4/Shh after suppression of PI3K/Cdk2/Smurf2 signaling. β-Actin served as a loading control. Notably, no changes in the expression of the aforementioned molecules were found in control astrocytes or mock-transduced astrocytes. mRNA expression was normalized to that of GAPDH mRNA. The results were obtained from three independent experiments. All data are reported as the means ± SEM. *$p < 0.05$, **$p < 0.01$, ***$p < 0.001$ versus the corresponding controls. GDC-0941 is a PI3K inhibitor, SU9516 a CDk2 inhibitor, and USF2 a Smurf2 inhibitor. CDk2, cyclin-dependent kinase 2; CTX, cortex; GLI2, GLI family zinc-finger 2; Nolz1, *Mus musculus* zinc-finger protein Nolz1; Ptch, patched homolog; Smurf2, Smad ubiquitin regulatory factor 2; Transd, transduction.

To our knowledge, this is the first report highlighting the generation of functional NSCs from mature astrocytes in one step with a single transcription factor (TF), casting doubt on the hypothesis that a certain single TF such as Sox2 and Ptfla is likely a master regulator of astrocyte reprogramming. Critically, Shh appears to be a very efficient enhancer of Oct4-mediated reprogramming of astrocytes into NSCs and displays strong activity in directly converting astrocytes into less differentiated NSCs. In addition, our present reprogramming of astrocytes into NSCs without lineage commitment switching thus validates neural functional specificity.

In previous studies on cell reprogramming, TF-mediated cell reprogramming has typically been favored and widely used because of its high efficiency and the relative simplicity of the implementation process. To date, several studies have achieved neural reprogramming by introducing neural-specific TFs into glial cells or other somatic cells.[28,30,32,34–36] Notwithstanding it is easy to obtain some somatic cells for reprogramming, such as fibroblasts, lineage switching is inevitable, thus resulting in a lack of functional specificity. In addition, it can be challenging to efficiently reprogram non-neural lineages into genuine NSCs. In previous studies, TF-mediated reprogramming usually involved the neural progenitor TFs Sox2, Oct4, Ascl1, and Ngn2, either separately or in combination with several other TFs,[29,30,32,37,38] leading to time consumption, tumorigenesis, as well as instability and uniformity of differentiation. Our present work has demonstrated that a single transcription factor, Oct4, in combination with a defined medium containing Shh is sufficient to generate NSCs from mature astrocytes. Due to the single

factor-mediated reprogramming, the chance of viral integration and further insertional mutagenesis is greatly reduced, and the converted NSCs will have higher levels of genomic stability than NSCs generated by multiple factors. Compared with the current increasing reports, the approach offers new promise that the repair of a damaged spinal cord can be achieved by cellular reprogramming with reduced numerous disadvantages mentioned earlier. First, our strategy reduces genome modification by minimizing the use of TF to a single factor, and thus facilitates therapeutic application for SCI and neurodegenerative diseases. This is mainly due to its unique molecular characteristics. It is reported that Oct4 drives a variety of pluripotent cell fate transcription regulators, effectors, and enhancers, as well as TFs by partnering with their DNA sequence at canonical binding sites.[39] The upregulation of Oct4 levels usually results in expression of pluripotency genes, maintenance of stemness, and self-renewal.[40] Thus, the Oct4-mediated cell reprogramming circumvents the future clinical risks and drawbacks of genome modification by use of a combination of multiple TFs and is likely to result in a less differentiated state. Second, Shh, a crucial factor, can effectively regulate cell proliferation and cell lineage-specific induction, and enhances efficiency of cell reprogramming. The present finding regarding Shh roles in astrocyte reprogramming is consistent with our previous study,[33] namely, the Shh pathway may directly participate in transcriptional activation of endogenous NSC master genes and regulation of downstream Gli2. Third, the reprogramming strategy is simple and easy to manipulate, bypassing the laborious approach of chemicals and multiple TFs. Therefore, successful reprogramming of astrocytes into iNSCs with Oct4 transduction in combination with Shh treatment may be safer than current strategies and may potentially lead to a novel drug therapy for SCI.

In this study, to substantiate our assumption and accurately determine the conversion efficiency, we first cultured mature astrocytes using a special method to eliminate astroglial intermediate progenitors because astroglial intermediate progenitors are easier to de-differentiate into NSCs. Our work revealed that the cultured astrocytes were positive for GFAP, GLT-1, and S100b, but not for neural progenitor and/or intermediate precursor markers, nestin, Pax6, CD133, Oligo2, and A2B5, strongly indicating that they were mature and not contaminated by other precursors in the starting astrocyte population. Therefore, these reprogrammed iNSCs undoubtedly originated from mature astrocytes without any contribution from other types of contaminating cells. Nevertheless, the primary astrocytes still may completely reflect their profiles *in vivo*. More rigorous culture strategy should be developed to exterminate certain controversy leading to more scientific claims. Notably, iNSCs obtained by Oct4-mediated direct reprogramming of astrocytes exhibited genuine NSC properties and tri-potential differentiation. The addition of Shh to Oct4-transduced astrocytes markedly enhanced the conversion efficiency, as demonstrated by the more rapid morphological changes, higher yield, and NSC marker expression, as well as subsequent higher differentiation efficiency *in vitro*. More strikingly, apart from the dramatic changes in cell-cycle distribution and cell proliferative capacity, the global gene expression patterns of iNSCs derived from astrocytes with Oct4 transduction and Shh stimulation were more similar to genuine NSCs than those of Oct4-transduced NSCs. By analyzing the differentially expressed genes, a more rapid transition from astrocytes toward NSCs in the treatment of Oct4/Shh than Oct4 alone was observed, confirming an easier acquisition of NSC identity. Lastly, the iNSCs from astrocytes induced by Oct4/Shh could differentiation into neurons with more specific functional characteristics as demonstrated by synapse formation, neuron Ca^{2+} imaging, and neurophysiology. To confirm this functionality, apart from Synapsin, PSD-95 and Homer1 expression were found at soma and neurites, indicating the formation of functional synapse. In line with this finding, the differentiated cells also possessed Ca^{2+} activity special for functional neurons. More importantly, they generated action potential and exhibited functional I_{Na} and I_k, as well as sPSCs. These findings further supported our previous results showing Oct4/Shh is critical for efficient reprogramming of astrocytes into genuine NSCs. Thus, our strategy allows the generation of iNSCs with key morphological, molecular, and functional features resembling those of wild-type NSCs at a large scale. Furthermore, the study also validates the crucial role of Shh signaling in Oct4 transcriptional regulation to remodel the epigenome and ultimately establish NSC fate.

Several lines of evidence have demonstrated that Oct4 is required in cell lineage-specific induction, fate determination, and maintenance of the pluripotent identity,[41,42] implying a critical role of Oct4 in the initial cell fate commitment during reprogramming. Our previous studies reveled that Shh is a key signal necessary for the astrocyte de-differentiation.[33] Likewise, Sirko et al.[43] also found that Shh is a key regulator of the stem cell response in reactive astrocytes. A more recent work also signified the importance of Shh in the conversion of astrocytes into other subtypes of cells by reprogramming.[44] These studies confirmed that Shh may act on a regulator of upstream astrocyte reprogramming and fate determination. Therefore, these further prompted us to generate NSCs by using an approach similar to those in recent study on the generation of NSCs through Shh and Oct4-mediated direct reprogramming. Based on our present findings, multiple mechanisms appear to be involved in this special combination-mediated reprogramming of NSCs from astrocytes. First, Sox2, a critical TF for triggering the reprogramming of somatic cells, was upregulated and activated. Specifically, it has been reported that in the presence of Shh, Sox2 selectively partners with Oct4 at a canonical binding site and forms a complex. The Oct4/Sox2 complex can regulate pluripotency and self-renewal genes, leading to cell-cycle re-entry and the further adoption of desirable fates.[39,45] Our *in vitro* analyses first showed that, following Oct4 transduction in combination with Shh stimulation, the levels of Oct4 and Sox2 were elevated exponentially, and the numbers and size of Sox2-positive neurospheres were markedly increased. Therefore, we speculated that the elevated expression of these two critical molecules in astrocytes may in part contribute to the molecular mechanism underlying the reversion of cell fate according to the above-mentioned together with the previous reports. However, the detailed signaling pathway that mediates the conversion of astrocytes into NSCs needs to be further elucidated.

Second, we further examined the expression of multiple signaling pathway components, including Ptc, Gli2, and CyclinD1, in this considerably complicated event. As expected, qPCR and western blot analyses showed that Ptc was significantly upregulated in Oct4- and Shh-treated astrocytes. Elevated Ptc expression greatly strengthens Shh signal transduction to Gli2, resulting in the transcription of certain molecules such as ErbB2, Wnt1, and Bmi1,[20,46,47] which are intimately associated with cell reprogramming, the disruption of cell-cycle arrest, cell-cycle re-entry, and cell lineage specification. Strikingly, similar expression patterns were found for the downstream transcription activator Gli2 and the effector CyclinD1, whereas no marked changes were detectable in normal astrocytes or astrocytes treated with Shh alone (data not shown). The finding is consistent with our previous reports that Shh is a key signal molecule necessary for initiating astrocyte reprogramming, suggesting that the activation of these signaling molecules is essential to elicit astrocyte reprogramming by Oct4 transduction in combination with Shh treatment.

Lastly, due to the complexity of the cell reprogramming event, there remains considerable interest in elucidating the possible mechanism of astrocyte reprogramming. Aside from the aforementioned molecules critical for differential modulation in astrocyte reversion, we found that Oct4 transduction of astrocytes combined with Shh treatment increased phos-PI3K and Cdk2 expression levels, indicating that the PI3K/Cdk2 signaling pathway may be involved in the reprogramming process, because the transition from G1 to G2 phase is rapidly initiated by translocation of the CDK2/cyclinD1 complex into the nucleus.[48,49] In addition, smurf2 was also activated during the conversion of astrocytes into NSCs. As documented previously, smurf2 activation is implicated in a wide range of cellular responses including cell proliferation, cell-cycle re-entry, epigenetic alteration, and migration.[50,51] More strikingly, Nolz1, a cell-cycle exit regulator,[52,53] was remarkably suppressed, which is in agreement with cell-cycle measurement. Another interesting finding was that a marked change in the expression of these molecules was found in Oct4-transduced astrocytes treated with Shh compared with mock, control, and Oct4-transduced astrocytes only. To substantiate our hypothesis, we used various combinations of three inhibitors, GDC-0941, NU9516, and USF2, to block the above-mentioned signaling pathways critical for cell-cycle re-entry, epigenetic regulation, cell proliferation, and cell fate commitment, etc. Intriguingly, the reprogramming of astrocytes induced by Oct4/Shh or Oct4 alone was remarkably suppressed, characterizing a drastic decrease in the levels of NSC-specific marker, and even no expression in some combinations. As to GFAP expression, no remarkable change was detectable (Figure 7E). Based on these results, we speculate that Oct4 and Shh elicit the reprogramming of astrocytes into NSCs through the collaboration of Sox2/Shh-mediated downstream signals and crosstalk with the PI3K/Cdk2/Smurf2 signaling pathway.

In conclusion, we underscore that a single TF, Oct4 in combination with Shh stimulation, can efficiently reprogram mature astrocytes into self-renewal and tripotent iNSCs albeit the existence of high heterogeneity in neural differentiation, thereby allowing large-scale functional neuron replenishment for treating SCI. This single factor-mediated astrocyte reprogramming is relatively safer and simpler than current strategies, which potentially reduces the chance of viral insertional mutagenesis and the risk for tumorigenesis. Regardless of the challenges, the reprogramming of astrocyte by single Oct4 in combination with the defined factor, Shh, provides a novel approach to generate NSCs. Specifically, the addition of Shh effectively potentiates Oct4-mediated reprogramming. Although the detailed molecular mechanism by which Oct4/Shh triggers astrocyte reprogramming still needs to be further investigated, our present results revealed that the reprogramming process is associated with the targeting of downstream signals by Sox2/Shh and PI3K/Cdk2/Smurf2, particularly with collaboration or crosstalk between these pathways, leading to epigenetic silencing of the GFAP gene, NSC specification, self-renewal, and stemness maintenance. In summary, our present strategy will provide the basis for future NSC generation and stem cell-based therapies for SCI and neurodegenerative disorders.

MATERIALS AND METHODS

Isolation and Culture of Spinal Cord Astrocytes

All experiments on animals were approved by the Animal Experimentation Ethics Committee of the National Academy of Science, and implemented according to the guidelines established by the Ministry of Health of China. Primary astrocytes were isolated from the spinal cords of 15-day-old Sprague-Dawley rats as described previously.[54] In brief, the mid-cervical to lumbar portions of the spinal cord were dissected and enzymatically dissociated into a single-cell suspension. The cells were then plated into poly-l-lysine (PLL)-coated, 25-cm^2 plastic flasks at a density of 1×10^5 cells/cm^2 in DMEM with 20% fetal calf serum (FCS), 2 mM glutamine, 25 mM HEPES, and penicillin and streptomycin. Half of the medium was refreshed once every 3 days. Ten days later, purification of the astrocytes was performed to exterminate non-astrocytes according to the protocol described by Yang et al.[54] After examination of astrocyte purity, cultures were maintained for the following experiments.

Neurosphere Cultures

Primary mature astrocytes were seeded at a density of 1×10^5 cells/cm^2 on PLL-coated six-well plates. The next days, the astrocytes were infected with the pGMLV-Oct4 virus in medium containing 8 μg/mL polybrene (production of Oct4 lentivirus is in the Supplemental Materials and Methods). After 24–36 h of infection, the viral supernatant was removed and refreshed with DF12 medium supplemented with 1% G5. At 2 days post-infection, the medium was switched to NSC culture medium (DF12 medium, 1% N2, 25 ng/mL basic fibroblast growth factor [bFGF], 20 ng/mL epidermal growth factor [EGF], penicillin and streptomycin). In parallel, Oct4-transduced cells were stimulated simultaneously with release of the microencapsulated Shh at a concentration of 20 ng/mL for 3, 7, 10, and 15 days. Thereafter, the floating neurospheres were mechanically isolated with a glass micropipette and subcultured with NSC culture medium. The neurospheres at passage 5 were further characterized. Notably, for the investigation of a possible mechanism underlying the

reprogramming event, three inhibitors, GDC-0941(a PI3K inhibitor) at 20 nM, SU9516 (a Cdk2 inhibitor) at 200 nM, and USF2 (Smurf2) at 1 μg/mL with different combinations, were administered into the reprogramming system and further maintained for 2–3 weeks for next experiments.

Immunofluorescence Staining

For immunostaining of each experimental group, all cultures were fixed with 4% paraformaldehyde for 15 min and permeabilized with Triton X-100 in PBS for 10 min, followed by incubation with 2% BSA and 5% corresponding secondary antibody serum in PBS for 1 h at room temperature. Primary antibodies were incubated with the specimens overnight at 4°C in 1% BSA in PBS. The following primary antibodies were used: goat anti-GFAP (1:1,000), rabbit anti-GLT-1 (1:1,500), mouse anti-nestin (1:1,000), mouse anti-Tuj-1 (1:1,500), rabbit anti-CNP (1:1,500), mouse anti-MAP2 (1:200), rabbit anti-GABA (1:200), goat anti-vGluT1 (1:100), rabbit anti-SYN (1:1,000), and goat anti-Sox2 (1:800). After the primary antibodies were removed and the samples were extensively washed with PBS three times, the secondary antibodies (Alexa Fluor 488/594 anti-mouse IgG, anti-rabbit IgG, and anti-goat IgG) were diluted in PBS and applied for 1 h in the dark at room temperature (antibody information is in the Supplemental Materials and Methods). The nuclei were counterstained with DAPI. Finally, the coverslips were mounted onto glass slides by using an anti-fading mounting medium. For investigation of *in vivo* differentiation of iNSCs, immunostaining of the spinal cord at 2–3 weeks after injection was performed according to the protocol described previously.[21] Finally, spinal cord sections were mounted onto glass for microscopy.

RT-PCR and qPCR Analysis

Total RNA was extracted using TRIzol reagent. Reverse transcription of 500 ng of total RNA was performed using a Prime Script Master Mix Kit (Takara) according to the manufacturer's protocol. The genes of interest were Oligo2, nestin, A2B5, CD133, Pax6, Tuj-1, GFAP, CNP, Sox2, Ptch, GLI2, Oct4, Blbp, Sox10, Nanog, Klf4, Zbtb48, Bmi, Hes5, stemness (STMN), transforming growth factor β (TGF-β), and CyclinD1. The housekeeping gene GAPDH was used as an internal control. The sequences of the primers used are listed in Table S1. The mRNA levels were quantified by SYBR Green-based quantitative real-time PCR (Takara) using an ABI Prism 7900 HT (Applied Biosystems). PCR was performed using standard procedures according to the manufacturer's instructions. The results were confirmed in at least three separate analyses.

Western Blots

The protein extract from cells with different treatments was collected, and western blotting was performed according to the protocol described previously.[21] Primary antibodies against the following proteins were used: Oct4, nestin, MAP2, vGluT1, GABA-T, GFAP, Pax6, CD133, Sox2, Tuj-1, CNP, SYN, PSD-95, Homer1, Ptch, GLI2, CyclinD1, Smurf2, Nolz1, Cdk2, and PI3K. All primary antibody dilutions were applied according to the manufacturer's instructions or minor adjustment. β-Actin was used as an internal control (notably, antibody information is in the Supplemental Materials and Methods). After thorough washes in PBS, the immunoblots were visualized using enhanced chemiluminescence and imaged using gel systems camera.

BrdU Incorporation Assay

The elevated proliferative ability of NSCs derived from astrocytes is an important feature of their self-renewal. To assess the proliferation of reprogrammed astrocytes at 3 and 7 days after Oct4 virus infection and treatment with Shh, BrdU (5 μM) was added to the culture medium and continuously maintained for 18 h. Subsequently, cells were fixed with 4% paraformaldehyde and treated with 2 N hydrochloric acid for 30 min at 37°C to denature DNA for further immunostaining. The immunostaining procedures were done as previously described.[55]

Flow Cytometry

Cell-cycle progression was determined by flow cytometry (Profile II; Coulter, Brea, CA, USA) according to a previously described protocol.[55] In brief, after astrocytes underwent the above-mentioned Oct4 virus infection and Shh treatment, the cells were trypsinized, triturated into single-cell suspensions, and further filtered through 80-μm nylon mesh prior to analysis. Concomitantly, the cells were fixed with 70% ethanol, incubated with 10 μL of RNase A (5 mg/mL) at 37°C for 30 min, and further stained with propidium iodide (100 mg/mL) for 30 min. The cells were then washed in PFN (PBS supplemented with 10% FCS and 0.02% sodium azide) thrice before flow cytometry analysis. The proliferation index (PI) was calculated and compared.

RNA-Seq Analysis

The global gene expression of the following cell populations was profiled by RNA-seq analysis: astrocytes, pri-NSCs, induced astrocytes (5 and 7 days after Oct4 induction), and induced astrocytes (5 and 7 days after Oct4 induction in conjugation with Shh). Total RNA of the cells from different treatment groups was isolated using an RNeasy mini kit (TaKaRa) according to the manufacturer's instructions. rRNA was depleted before RNA-seq library preparation. The prepared libraries were sequenced using an Illumina HiSeq3000 sequencer (Wuhan Kangce Biotechnology Corporation, China). Subsequent procedures were undertaken as described previously.[18] The obtained sequence reads were trimmed and mapped to the rat reference genome using TopHat, and gene expression and expression changes were analyzed using Cufflinks. Scatterplots of gene expression levels were carried out as previously described.[34] The biosample accession number for the RNA-seq data file reported in this study is SAMN11523986. In addition, we included Bioproject number of raw sequence reads: PRJNA534182 and SRA metadata accession number SRR9021096-SRR9021101.

In Vitro and *In Vivo* Cell Differentiation

To assess the functional ability of NSCs derived from astrocytes to differentiate into neurons and glial cells, neurospheres were treated according to our previously published method.[21] For *in vitro* cell differentiation, neurospheres were harvested, plated on PLL-coated

coverslips, and maintained in Neurobasal medium containing 2% B27 and 4 μM retinoic acid (RA). Following 2 days of incubation, brain-derived neurotrophic factor (BDNF; 20 ng/mL), nerve growth factor (NGF; 25 ng/mL), and 2% FBS were added into the cultures to further induce cell differentiation. The cells were then maintained in culture for over 2 weeks. To analyze the differentiation of iNSCs *in vivo*, the above harvested neurospheres were first labeled with CMFDA for 20 min according to the manufacturer's instructions, washed thrice with Hank's solution, and isolated into a single-cell suspension. The CMFDA-labeling cells (totally 5×10^5 cells) were injected into the spinal cord region (T8–T9) of 2-month-old Sprague-Dawley rats using 10-μL syringes. Notably, the injection speed at a rate of 1 μL/min was executed, and syringes should keep for an additional 5 min to prevent leakage upon withdrawal. After 2 weeks or longer, the coverslips with differentiated cells and the spinal cords were then collected for double-immunofluorescent staining and functional assessment. Eventually, their neural differentiation was compared, and cell counts were performed by observers blinded to the experiments.

Electrophysiology

After induction of astrocyte-derived NSCs for 3 weeks, the differentiated cells were transferred to artificial cerebrospinal fluid (ACSF) and bubbled with 95% O_2 and 5% CO_2 for assessment of their cell ability to fire action potentials. The ACSF was made as previously described.[56] Whole-cell patch-clamp experiments were performed at 20°C–22°C under an inverted microscope (Zeiss, Jena, Germany). For current-clamp recordings, we applied current pulses with a step size of 10 pA to test the ability to generate action potentials. Cells with leak currents <100 pA were used for further analysis. Whole-cell currents were low-pass filtered at 2.9 kHz, digitized at 10 kHz using an EPC-10 amplifier (HEKA, Lambrecht, Germany), and analyzed with PATCHMASTER (HEKA). TTX (0.2 μM; Sigma-Aldrich) was diluted in the bath solution and applied via gravity using a SF-77B perfusion fast-step system as described previously.[57] Whole-cell sodium and potassium currents were elicited and recorded in voltage-clamp mode in response to a series of voltage steps ranging from −50 to +50 mV at 10-mV increments. sPSCs were recorded in voltage-step mode. In all voltage-clamp recordings, cells were clamped at −50 or −70 Mv (n = 20). Finally, data were analyzed using pClamp9 Clampfit software and MiniAnalysis software.

Calcium Imaging

To determine whether neuronal cells derived from reprogrammed astrocytes are functional, we assessed calcium influx in individual cells as previously described.[58] In brief, at 7 and 10 days post-Oct4 transduction in the presence or absence of Shh, the reprogrammed cells were further induced for 3 weeks using the aforementioned conditions. Concomitantly, the differentiated cells were transferred to Neurobasal medium containing 1% B27 and 2 μM calcium ion-sensitive fluorescent indicator Fluo 2-AM (Sigma-Aldrich) and maintained for 30 min at 37°C. After fully washing twice in a perfusion chamber with extracellular medium (EM; 140 mM NaCl, 2 mM $CaCl_2$, 5 mM KCl, 10 mM HEPES, and 10 mM glucose, adjusted to pH 7.2–7.4), calcium imaging was conducted in EM with Zeiss LSM 710 confocal microscopy. To specifically determine the Ca^{2+} influx, a Ca^{2+} channel activator (10 μM BayK; Stemgent) or blocker (5 μM nifedipine; Sigma-Aldrich) was added to the cultures to observe the changes in the Ca^{2+} influx images. The whole procedure was executed according to our previous report.[59] To further characterize their physiological profiling of the induced neurons, KCl at 100 mM was added into cells following nifedipine treatment. Subsequently, the Ca^{2+} influx images were conducted and analyzed according to the aforementioned procedure.

Cell Counts and Statistical Analysis

Cell counts were performed by observing 15 randomly selected views per coverslip with a fluorescent microscope under ×20 magnification. Each observation field is approximately 0.45 mm^2. Neurosphere counts were performed as previously described after cultures were terminated at each time point.[60] A total of four coverslips for each group were used for count analyses. Notably, to discriminate between the experimental and control groups, counting was done in duplicate according to the same counting criterion by a person without knowledge of the experiment. For all analyses, the values are expressed as the mean ± SEM from at least three independent experiments. Statistical analysis was performed using the statistical software SPSS 10.0. ANOVA was used to analyze significant differences among groups under different conditions, and $p < 0.05$ was considered statistically significant.[55]

SUPPLEMENTAL INFORMATION

Supplemental Information can be found online at https://doi.org/10.1016/j.ymthe.2019.05.006.

AUTHOR CONTRIBUTIONS

H.Y. conceived the study and designed the work. D. Hao, C.L., B.C., D. Huang, L.Z., Q.Z., Y.W., and J.A. performed cellular and molecular experiments, and collected and analyzed data. H.F. performed the *in vitro* electrophysiology experiments and cell microinjection. D. Hao, C.L., B.C., Q.Z., J.Z., and H.Y. performed data analysis and interpretation. D. Hao and H.Y. wrote the manuscript.

CONFLICTS OF INTEREST

The authors declare no competing interests.

ACKNOWLEDGMENTS

This work was supported by the Natural Science Foundation of China (grants 81571208, 81772357, and 81472098), a key grant from the National Nature Science Foundation of China (81830077), the Natural Science Foundation of Shaanxi province (grant 2017JM8012), and a key fund of Honghui Hospital (YJ2017001). The authors confirm that there has been no financial support for this research that could have influenced it.

REFERENCES

1. Johnstone, V.P., Wright, D.K., Wong, K., O'Brien, T.J., Rajan, R., and Shultz, S.R. (2015). Experimental traumatic brain injury results in long-term recovery of functional responsiveness in sensory cortex but persisting structural changes and sensorimotor, cognitive, and emotional deficits. J. Neurotrauma *32*, 1333–1346.

2. Mattson, M.P. (2000). Apoptosis in neurodegenerative disorders. Nat. Rev. Mol. Cell Biol. *1*, 120–129.
3. Bhowmick, S., D'Mello, V., Ponery, N., and Abdul-Muneer, P.M. (2018). Neurodegeneration and sensorimotor deficits in the mouse model of traumatic brain Injury. Brain Sci. *8*, E11.
4. Carreon, L.Y., and Dimar, J.R. (2011). Early versus late stabilization of spine injuries: a systematic review. Spine *36*, E727–E733.
5. Vismara, I., Papa, S., Rossi, F., Forloni, G., and Veglianese, P. (2017). Current options for cell therapy in spinal cord injury. Trends Mol. Med. *23*, 831–849.
6. Baptiste, D.C., and Fehlings, M.G. (2007). Update on the treatment of spinal cord injury. Prog. Brain Res. *161*, 217–233.
7. Lepore, A.C., Neuhuber, B., Connors, T.M., Han, S.S.W., Liu, Y., Daniels, M.P., Rao, M.S., and Fischer, I. (2006). Long-term fate of neural precursor cells following transplantation into developing and adult CNS. Neuroscience *142*, 287–304.
8. Martínez-Serrano, A., and Björklund, A. (1997). Immortalized neural progenitor cells for CNS gene transfer and repair. Trends Neurosci. *20*, 530–538.
9. Pessina, A., and Gribaldo, L. (2006). The key role of adult stem cells: therapeutic perspectives. Curr. Med. Res. Opin. *22*, 2287–2300.
10. Gruen, L., and Grabel, L. (2006). Concise review: scientific and ethical roadblocks to human embryonic stem cell therapy. Stem Cells *24*, 2162–2169.
11. Swijnenburg, R.J., Schrepfer, S., Govaert, J.A., Cao, F., Ransohoff, K., Sheikh, A.Y., Haddad, M., Connolly, A.J., Davis, M.M., Robbins, R.C., and Wu, J.C. (2008). Immunosuppressive therapy mitigates immunological rejection of human embryonic stem cell xenografts. Proc. Natl. Acad. Sci. USA *105*, 12991–12996.
12. Ben-David, U., and Benvenisty, N. (2011). The tumorigenicity of human embryonic and induced pluripotent stem cells. Nat. Rev. Cancer *11*, 268–277.
13. Heine, V.M., Dooves, S., Holmes, D., and Wagner, J. (2012). Reprogramming: a new era in regenerative medicine. In Induced Pluripotent Stem Cells in Brain Diseases (Springer Briefs in Neuroscience), pp. 1–25.
14. Mertens, J., Marchetto, M.C., Bardy, C., and Gage, F.H. (2016). Evaluating cell reprogramming, differentiation and conversion technologies in neuroscience. Nat. Rev. Neurosci. *17*, 424–437.
15. Kim, S.M., Flaßkamp, H., Hermann, A., Araúzo-Bravo, M.J., Lee, S.C., Lee, S.H., Seo, E.H., Lee, S.H., Storch, A., Lee, H.T., et al. (2014). Direct conversion of mouse fibroblasts into induced neural stem cells. Nat. Protoc. *9*, 871–881.
16. Han, D.W., Tapia, N., Hermann, A., Hemmer, K., Höing, S., Araúzo-Bravo, M.J., Zaehres, H., Wu, G., Frank, S., Moritz, S., et al. (2012). Direct reprogramming of fibroblasts into neural stem cells by defined factors. Cell Stem Cell *10*, 465–472.
17. Lujan, E., Chanda, S., Ahlenius, H., Südhof, T.C., and Wernig, M. (2012). Direct conversion of mouse fibroblasts to self-renewing, tripotent neural precursor cells. Proc. Natl. Acad. Sci. USA *109*, 2527–2532.
18. Zhang, M., Lin, Y.H., Sun, Y.J., Zhu, S., Zheng, J., Liu, K., Cao, N., Li, K., Huang, Y., and Ding, S. (2016). Pharmacological reprogramming of fibroblasts into neural stem cells by signaling-directed transcriptional activation. Cell Stem Cell *18*, 653–667.
19. Zhu, S., Wang, H., and Ding, S. (2015). Reprogramming fibroblasts toward cardiomyocytes, neural stem cells and hepatocytes by cell activation and signaling-directed lineage conversion. Nat. Protoc. *10*, 959–973.
20. Yang, H., Ling, W., Vitale, A., Olivera, C., Min, Y., and You, S. (2011). ErbB2 activation contributes to de-differentiation of astrocytes into radial glial cells following induction of scratch-insulted astrocyte conditioned medium. Neurochem. Int. *59*, 1010–1018.
21. Feng, G.D., He, B.R., Lu, F., Liu, L.H., Zhang, L., Chen, B., He, Z.P., Hao, D.J., and Yang, H. (2014). Fibroblast growth factor 4 is required but not sufficient for the astrocyte dedifferentiation. Mol. Neurobiol. *50*, 997–1012.
22. Ben Haim, L., and Rowitch, D.H. (2017). Functional diversity of astrocytes in neural circuit regulation. Nat. Rev. Neurosci. *18*, 31–41.
23. Takuma, K., Baba, A., and Matsuda, T. (2004). Astrocyte apoptosis: implications for neuroprotection. Prog. Neurobiol. *72*, 111–127.
24. Chang, M.L., Wu, C.H., Jiang-Shieh, Y.F., Shieh, J.Y., and Wen, C.Y. (2007). Reactive changes of retinal astrocytes and Müller glial cells in kainate-induced neuroexcitotoxicity. J. Anat. *210*, 54–65.
25. Shin, Y.J., Kim, H.L., Park, J.M., Cho, J.M., Kim, S.Y., and Lee, M.Y. (2013). Characterization of nestin expression and vessel association in the ischemic core following focal cerebral ischemia in rats. Cell Tissue Res. *351*, 383–395.
26. Lang, B., Liu, H.L., Liu, R., Feng, G.D., Jiao, X.Y., and Ju, G. (2004). Astrocytes in injured adult rat spinal cord may acquire the potential of neural stem cells. Neuroscience *128*, 775–783.
27. Steindler, D.A., and Laywell, E.D. (2003). Astrocytes as stem cells: nomenclature, phenotype, and translation. Glia *43*, 62–69.
28. Wang, C., Fong, H., and Huang, Y. (2015). Direct reprogramming of RESTing astrocytes. Cell Stem Cell *17*, 1–3.
29. Corti, S., Nizzardo, M., Simone, C., Falcone, M., Donadoni, C., Salani, S., Rizzo, F., Nardini, M., Riboldi, G., Magri, F., et al. (2012). Direct reprogramming of human astrocytes into neural stem cells and neurons. Exp. Cell Res. *318*, 1528–1541.
30. Niu, W., Zang, T., Smith, D.K., Vue, T.Y., Zou, Y., Bachoo, R., Johnson, J.E., and Zhang, C.L. (2015). SOX2 reprograms resident astrocytes into neural progenitors in the adult brain. Stem Cell Reports *4*, 780–794.
31. Gao, L., Guan, W., Wang, M., Wang, H., Yu, J., Liu, Q., Qiu, B., Yu, Y., Ping, Y., Bian, X., et al. (2017). Direct generation of human neuronal cells from adult astrocytes by small molecules. Stem Cell Reports *8*, 538–547.
32. Guo, Z., Zhang, L., Wu, Z., Chen, Y., Wang, F., and Chen, G. (2014). In vivo direct reprogramming of reactive glial cells into functional neurons after brain injury and in an Alzheimer's disease model. Cell Stem Cell *14*, 188–202.
33. Yang, H., Feng, G.D., Olivera, C., Jiao, X.Y., Vitale, A., Gong, J., and You, S.W. (2012). Sonic hedgehog released from scratch-injured astrocytes is a key signal necessary but not sufficient for the astrocyte de-differentiation. Stem Cell Res. (Amst.) *9*, 156–166.
34. Xiao, D., Liu, X., Zhang, M., Zou, M., Deng, Q., Sun, D., Bian, X., Cai, Y., Guo, Y., Liu, S., Li, S., et al. (2018). Direct reprogramming of fibroblasts into neural stem cells by single non-neural progenitor transcription factor Ptf1a. Nat. Commun. *9*, 2865.
35. Mai, T., Markov, G.J., Brady, J.J., Palla, A., Zeng, H., Sebastiano, V., and Blau, H.M. (2018). NKX3-1 is required for induced pluripotent stem cell reprogramming and can replace OCT4 in mouse and human iPSC induction. Nat. Cell Biol. *20*, 900–908.
36. Yang, N., Ng, Y.H., Pang, Z.P., Südhof, T.C., and Wernig, M. (2011). Induced neuronal cells: how to make and define a neuron. Cell Stem Cell *9*, 517–525.
37. Heinrich, C., Blum, R., Gascón, S., Masserdotti, G., Tripathi, P., Sánchez, R., Tiedt, S., Schroeder, T., Götz, M., and Berninger, B. (2010). Directing astroglia from the cerebral cortex into subtype specific functional neurons. PLoS Biol. *8*, e1000373.
38. Liu, M.L., Zang, T., Zou, Y., Chang, J.C., Gibson, J.R., Huber, K.M., and Zhang, C.L. (2013). Small molecules enable neurogenin 2 to efficiently convert human fibroblasts into cholinergic neurons. Nat. Commun. *4*, 2183.
39. Mansour, A.A., and Hanna, J.H. (2013). Oct4 shuffles Sox partners to direct cell fate. EMBO J. *32*, 917–919.
40. Chambers, I., and Smith, A. (2004). Self-renewal of teratocarcinoma and embryonic stem cells. Oncogene *23*, 7150–7160.
41. Le Bin, G.C., Muñoz-Descalzo, S., Kurowski, A., Leitch, H., Lou, X., Mansfield, W., Etienne-Dumeau, C., Grabole, N., Mulas, C., Niwa, H., et al. (2014). Oct4 is required for lineage priming in the developing inner cell mass of the mouse blastocyst. Development *141*, 1001–1010.
42. Wang, H., Cao, N., Spencer, C.I., Nie, B., Ma, T., Xu, T., Zhang, Y., Wang, X., Srivastava, D., and Ding, S. (2014). Small molecules enable cardiac reprogramming of mouse fibroblasts with a single factor, Oct4. Cell Rep. *6*, 951–960.
43. Sirko, S., Behrendt, G., Johansson, P.A., Tripathi, P., Costa, M., Bek, S., Heinrich, C., Tiedt, S., Colak, D., Dichgans, M., et al. (2013). Reactive glia in the injured brain acquire stem cell properties in response to sonic hedgehog. Cell Stem Cell *12*, 426–439.
44. Petrova, R., Garcia, A.D., and Joyner, A.L. (2013). Titration of GLI3 repressor activity by sonic hedgehog signaling is critical for maintaining multiple adult neural stem cell and astrocyte functions. J. Neurosci. *33*, 17490–17505.
45. Aksoy, I., Jauch, R., Chen, J., Dyla, M., Divakar, U., Bogu, G.K., Teo, R., Leng Ng, C.K., Herath, W., Lili, S., et al. (2013). Oct4 switches partnering from Sox2 to Sox17 to reinterpret the enhancer code and specify endoderm. EMBO J. *32*, 938–953.
46. Liu, Y., and Rao, M.S. (2004). Glial progenitors in the CNS and possible lineage relationships among them. Biol. Cell *96*, 279–290.

47. Sher, F., Boddeke, E., and Copray, S. (2011). Ezh2 expression in astrocytes induces their dedifferentiation toward neural stem cells. Cell. Reprogram. *13*, 1–6.

48. Keenan, S.M., Bellone, C., and Baldassare, J.J. (2001). Cyclin-dependent kinase 2 nucleocytoplasmic translocation is regulated by extracellular regulated kinase. J. Biol. Chem. *276*, 22404–22409.

49. Min, J., Singh, S., Fitzgerald-Bocarsly, P., and Wood, T.L. (2012). Insulin-like growth factor I regulates G2/M progression through mammalian target of rapamycin signaling in oligodendrocyte progenitors. Glia *60*, 1684–1695.

50. Brandenberger, R., Wei, H., Zhang, S., Lei, S., Murage, J., Fisk, G.J., Li, Y., Xu, C., Fang, R., Guegler, K., et al. (2004). Transcriptome characterization elucidates signaling networks that control human ES cell growth and differentiation. Nat. Biotechnol. *22*, 707–716.

51. Lin, X., Liang, M., and Feng, X.H. (2000). Smurf2 is a ubiquitin E3 ligase mediating proteasome-dependent degradation of Smad2 in transforming growth factor-beta signaling. J. Biol. Chem. *275*, 36818–36822.

52. Chang, C.W., Tsai, C.W., Wang, H.F., Tsai, H.C., Chen, H.Y., Tsai, T.F., Takahashi, H., Li, H.Y., Fann, M.J., Yang, C.W., et al. (2004). Identification of a developmentally regulated striatum-enriched zinc-finger gene, Nolz-1, in the mammalian brain. Proc. Natl. Acad. Sci. USA *101*, 2613–2618.

53. Urbán, N., Martín-Ibáñez, R., Herranz, C., Esgleas, M., Crespo, E., Pardo, M., Crespo-Enríquez, I., Méndez-Gómez, H.R., Waclaw, R., Chatzi, C., et al. (2010). Nolz1 promotes striatal neurogenesis through the regulation of retinoic acid signaling. Neural Dev. *5*, 21.

54. Yang, H., Liang, Z., Li, J., Cheng, X., Luo, N., and Ju, G. (2006). Optimized and efficient preparation of astrocyte cultures from rat spinal cord. Cytotechnology *52*, 87–97.

55. Hao, D.J., Liu, C., Zhang, L., Chen, B., Zhang, Q., Zhang, R., An, J., Zhao, J., Wu, M., Wang, Y., et al. (2017). Lipopolysaccharide and curcumin co-stimulation potentiates olfactory ensheathing cell phagocytosis via enhancing their activation. Neurotherapeutics *14*, 502–518.

56. Yang, H., Liu, Y., Hai, Y., Guo, Y., Yang, S., Li, Z., Gao, W.Q., and He, Z. (2015). Efficient conversion of spermatogonial stem cells to phenotypic and functional dopaminergic neurons via the PI3K/Akt and P21/Smurf2/Nolz1 Pathway. Mol. Neurobiol. *52*, 1654–1669.

57. Son, E.Y., Ichida, J.K., Wainger, B.J., Toma, J.S., Rafuse, V.F., Woolf, C.J., and Eggan, K. (2011). Conversion of mouse and human fibroblasts into functional spinal motor neurons. Cell Stem Cell *9*, 205–218.

58. Xu, H., Wang, Y., He, Z., Yang, H., and Gao, W.Q. (2015). Direct conversion of mouse fibroblasts to GABAergic neurons with combined medium without the introduction of transcription factors or miRNAs. Cell Cycle *14*, 2451–2460.

59. Tropel, P., Platet, N., Platel, J.C., Noël, D., Albrieux, M., Benabid, A.L., and Berger, F. (2006). Functional neuronal differentiation of bone marrow-derived mesenchymal stem cells. Stem Cells *24*, 2868–2876.

60. Hunt, J., Cheng, A., Hoyles, A., Jervis, E., and Morshead, C.M. (2010). Cyclosporin A has direct effects on adult neural precursor cells. J. Neurosci. *30*, 2888–2896.

YMTHE, Volume *27*

Supplemental Information

Sonic Hedgehog Effectively Improves Oct4-Mediated Reprogramming of Astrocytes into Neural Stem Cells

Hao Yang, Cuicui Liu, Hong Fan, Bo Chen, Dageng Huang, Lingling Zhang, Qian Zhang, Jing An, Jingjing Zhao, Yi Wang, and Dingjun Hao

Supplemental Information

1. Supplemental data

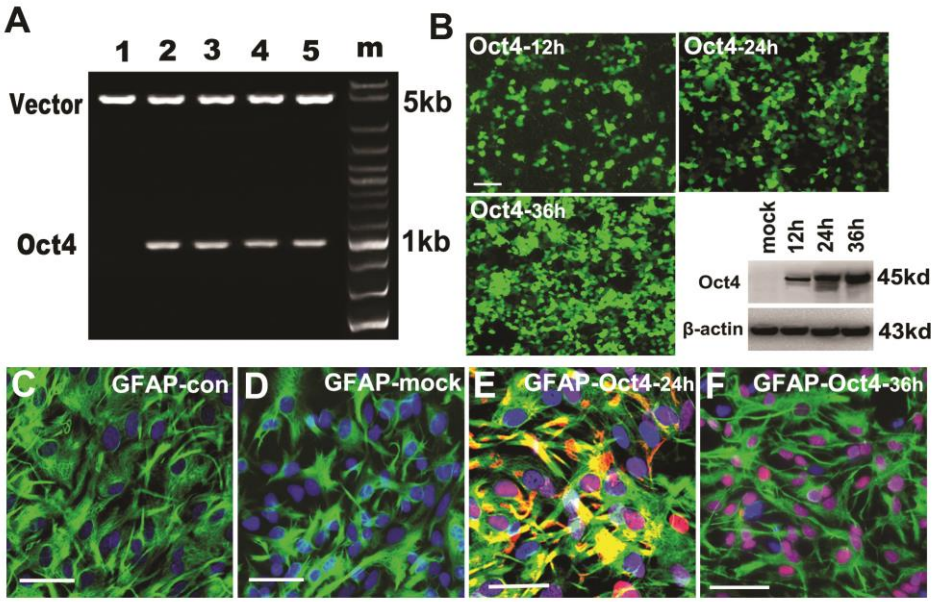

Figure S1 Identification of the Oct4 lentiviral vector and transduction of astrocytes. (A) The recombinant Oct4-pGMLV lentiviral vector from four clones was identified by restriction endonuclease digestion. (B) Identification of Oct4 expression in 293T cells transfected with Oct4 lentiviral vector for 12, 24, and 36 h, no immunostaining photomicrographs are shown for the mock-transfected cells, since Oct4 expression was undetectable in these cells. (C) Untransduced astrocytes. (D) Astrocytes infected with mock lentiviral vector. (E, F) Astrocytes infected with lentivirus encoding Oct4 for 24 and 36 h. Scale bars=100 μm.

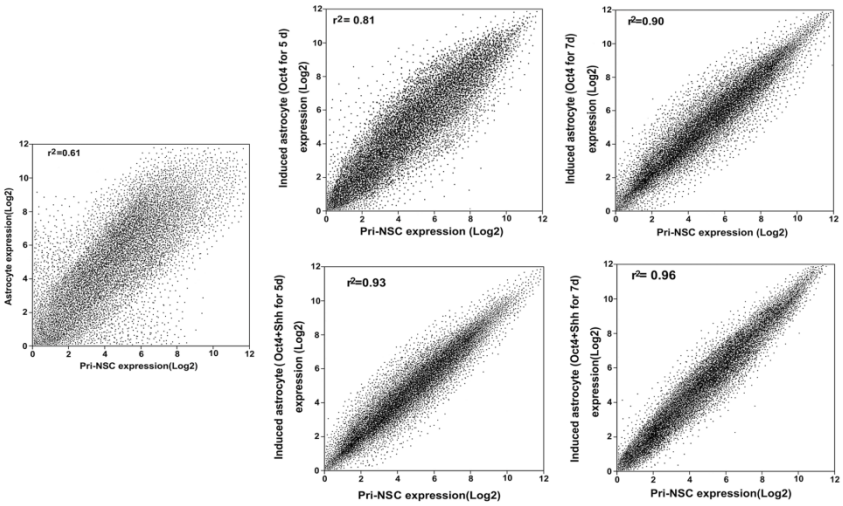

Figure S2 Correlation of Scatterplot analysis of global gene expression profiles of primary NSCs, induced astrocytes with Oct4/Shh or Oct4 alone, and astrocytes. The gene expression levels are indicated on a Log2 scale. Pearson's correlation coefficients (r) are indicated.

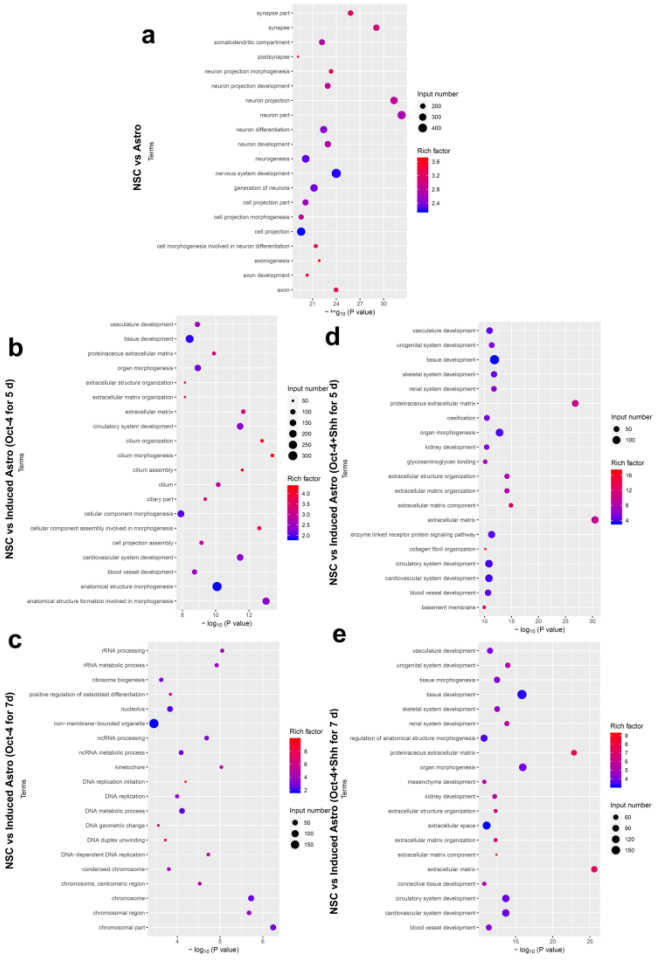

Figure S3 Gene ontology (GO) enrichment analysis of the upregulated genes between

primary NSC and induced astrocytes with Oct4/Shh or Oct4 alone or astrocytes. The upregulated genes were analyzed for enrichment by gene-set enrichment analysis. (a) Enrichment analysis of the upregulated genes between astrocyte and primary NSCs. (b-c) Enrichment analysis of the upregulated genes between induced astrocytes (Oct4 for 5d and 7d, respectively) and primary NSCs. Green represents GFAP. (d-e) Enrichment analysis of the upregulated genes between induced astrocytes (Oct4+Shh for 5d and 7d, respectively) and primary NSCs. Green represents GFAP, red represents Oct4.

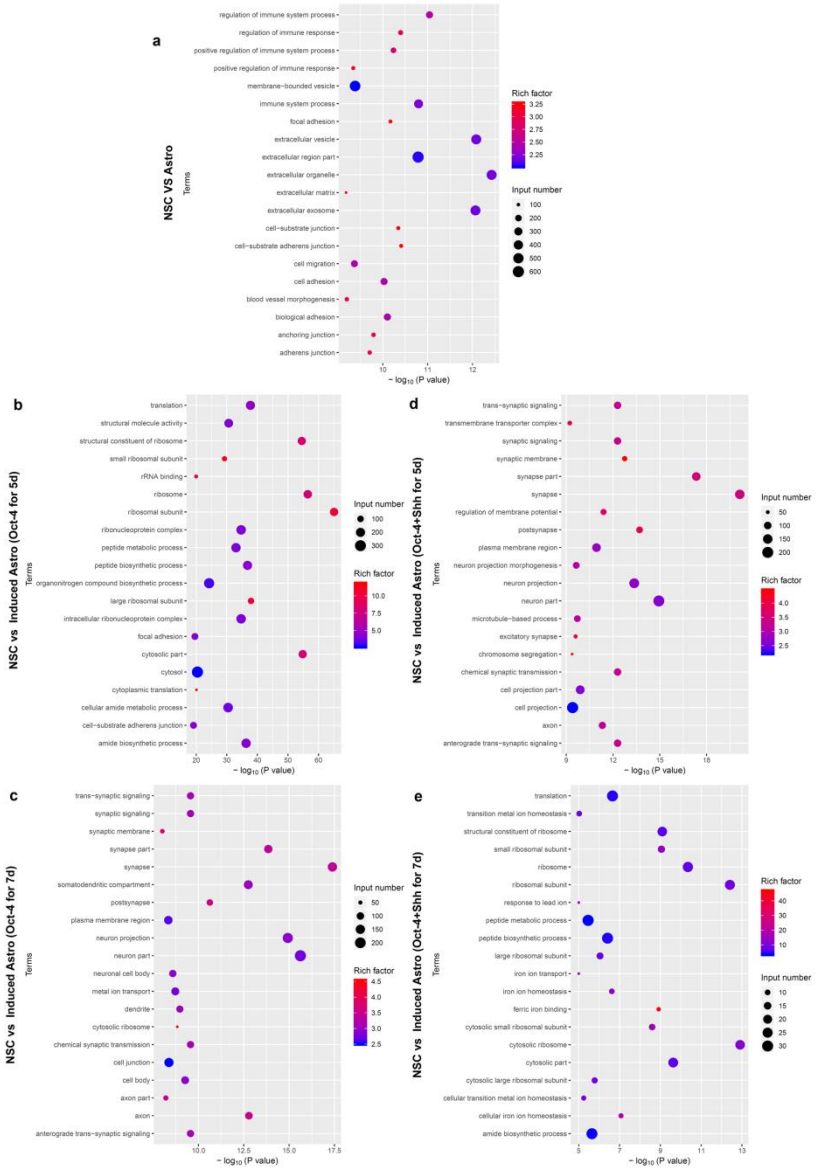

Figure S4 Gene ontology (GO) enrichment analysis of the downregulated genes between primary NSC and induced astrocytes with Oct4/Shh or Oct4 alone or

astrocytes. (a) Enrichment analysis of the downregulated genes between astrocyte and primary NSCs. (b-c) Enrichment analysis of the downregulated genes between induced astrocytes (Oct4 for 5d and 7d, respectively) and primary NSCs. (b-c) Enrichment analysis of the downregulated genes between induced astrocytes (Oct4+Shh for 5d and 7d, respectively) and primary NSCs.

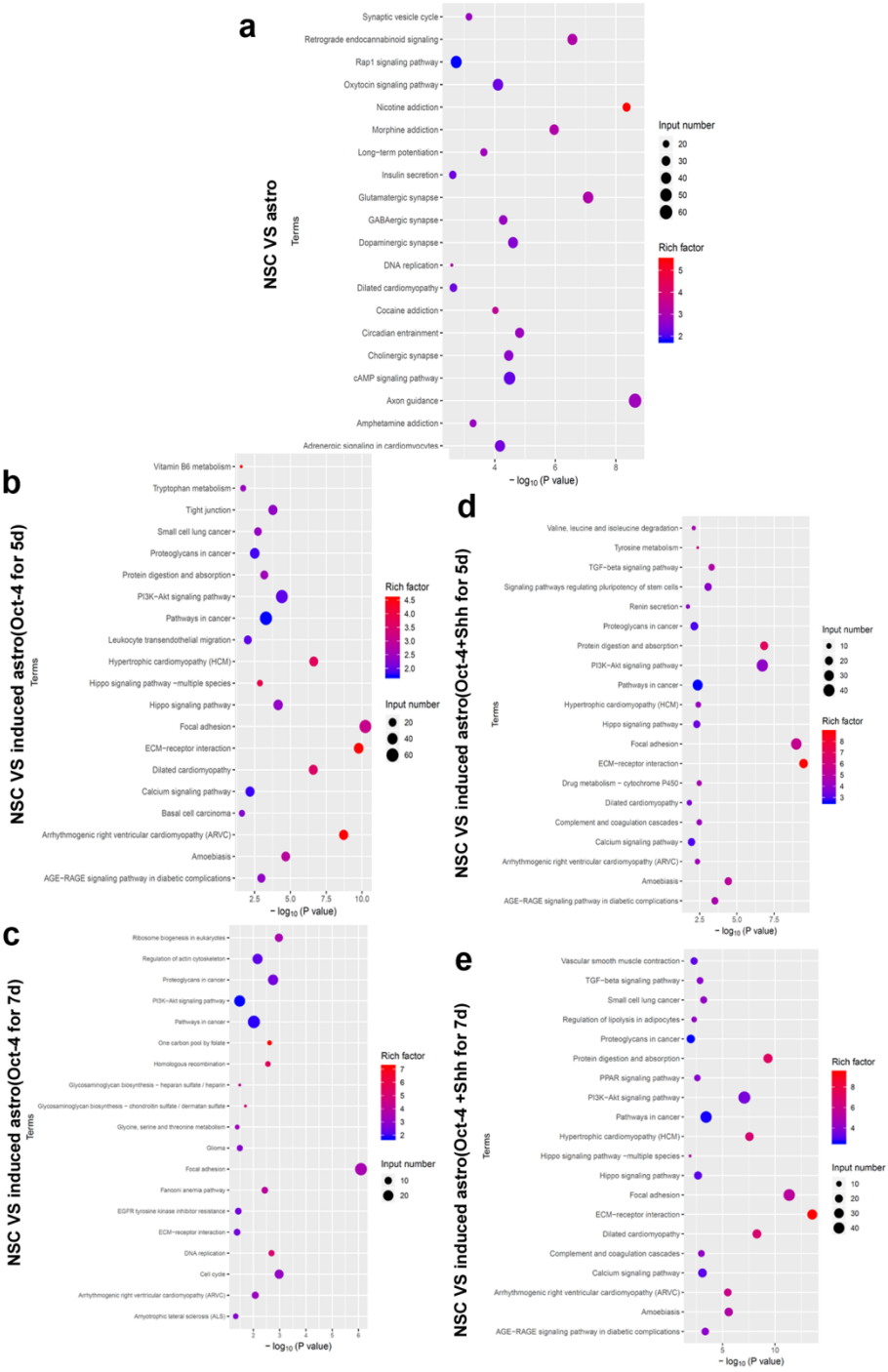

Figure S5 Gene ontology (GO) enrichment analysis of the upregulated genes for

KEGG pathway between primary NSCs and induced astrocytes with Oct4/Shh or Oct4 alone or astrocytes. (a) The upregulated genes for KEGG pathway between astrocyte and primary NSCs. (b-c) The upregulated genes for KEGG pathway between induced astrocytes (Oct4 for 5d and 7d, respectively) and primary NSCs. (d-e) The upregulated genes for KEGG pathway between induced astrocytes (Oct4+Shh for 5d and 7d, respectively) and primary NSCs.

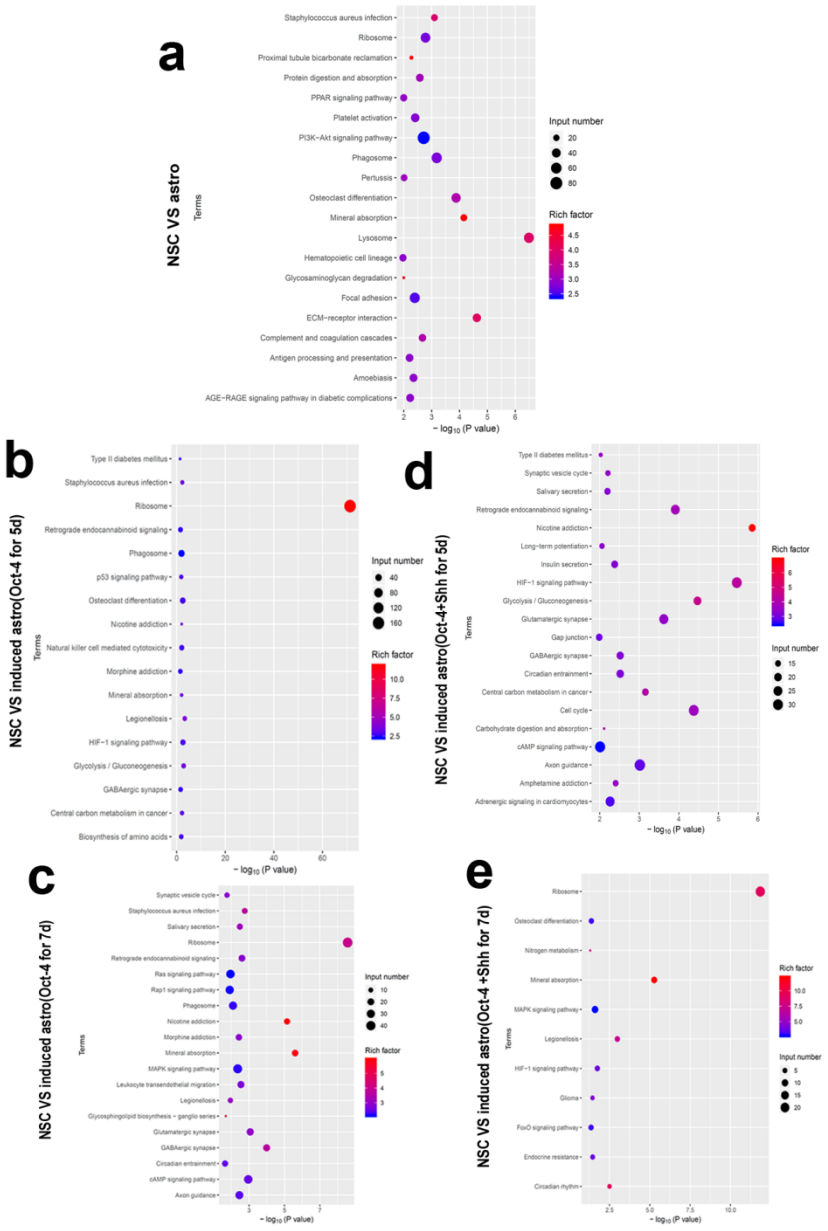

Figure S6 Gene ontology (GO) enrichment analysis of the downregulated genes for KEGG pathway between primary NSCs and induced astrocytes with Oct4/Shh or Oct4 alone or astrocytes. (a) The downregulated genes for KEGG pathway between

astrocyte and primary NSCs. (b-c) The downregulated genes for KEGG pathway between induced astrocytes (Oct4 for 5d and 7d, respectively) and primary NSCs. (d-e) The downregulated genes for KEGG pathway between induced astrocytes (Oct4+Shh for 5d and 7d, respectively) and primary NSCs.

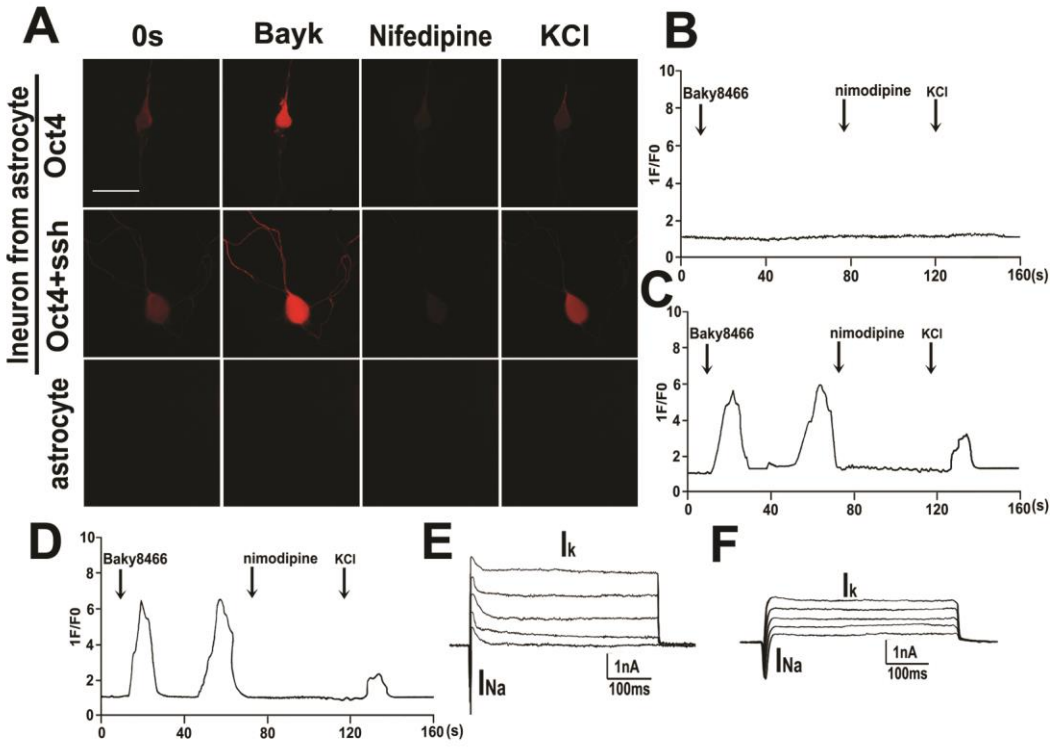

Figure S7 Functional characteristics of the neurons derived from induced astrocytes with Oct4 and Shh. (A) Changes in the calcium response in astrocytes or differentiated neurons derived from iNSCs (induced with Oct4 alone, or with Oct4/Shh) with the indicated treatments. Scale bars=25μl (B-D) the ratio of the cell fluorescence intensity at the indicated time to the fluorescence intensity of the above-mentioned astrocytes, differentiated neurons from iNSCs induced with Oct4 alone, and with Oct4 and Shh, respectively. BayK (10 mM), nifedipine (5 mM), KCl (100 mM) administered at the indicated time points. (E-F) Representative traces showing Na^+ and K^+ current recorded from differentiated neurons derived from iNSCs induced with Oct4/Shh with Oct4 alone. The total number of cells tested in each experiment was approximately 10; representative results are presented.

Table S1 The sequences of primer sets used for RT-PCR and QPCR analysis.

Primer sets used for RT-PCR and qPCR

Gene	Forward primer	Reverse primer
Nestin	5′-TGCAGCCACTGAGGTATCTG-3′	5′-CAGTTCCCACTCCTGTGGTT-3′
Olig2	5′-GGCGGTGGCTTCAAGTCATC-3′	5′-TAGTTTCGCGCCAGCAGCAG-3′
CD133	5′-CTTGGCATCGCGTTTGG-3′	5′-GAGCCCGCAAGTCTCTGTAATT-3′
Pax6	5′-GGCAACCTACGCAAGATGGC-3′	5′-TGAGGGCTGTGTCTGTTCGG-3′
A2B5	5′-ACATCGAGATCGCCACCTAC-3′	5′ -ACATCACATCCTTGTGCTCC-3′
GFAP	5′-GCGCTCAATGCTGGCTTCAA-3′	5′-ACGCAGCCAGGTTGTTCTCT-3′
Oct4	5′-CGTTCTCTTTGGAAAGGTGTTC-3′	5′-ACACTCGGACCACGTCTTTC-3′
Sox2	5′-GCAGTACAACTCCATGAC-3′	5′-CGAGTAGGACATGCTGTA-3′
Ptc	5-AACAAAAATTCAACCAAACCTC-3′	5′-TGTCTTCATTCCAGTTGATGTG-3
GLI2	5′-CGCCTGGAGAACTTGAAGAC-3′	5′-TTCTCATTGGAGTGAGTGCG-3′
CyclinD1	5′-CTCCCCACGATTTCATCGAA-3′	5′-GTGCATGTTTGCGGATGATC-3′
BLBP	5′-AGGGCAAGGATGGTAGATGC-3′	5′-ACCGTTGTTTTGGTCACATT-3′
Sox10	5′-GCTGAACGAGAGTGACAAGC-3′	5′-ATGGGCTGATCTCCCCGATGT-3′
Nanog	5′-TCTCCTCCGCCTTCCTCT-3′	5′-TTGCCTCTGAAACCTATCCTTG-3′
Klf4	5′-AGGAGCCCCAAGCCAAAGAG-3′	5′-ACAAGTGTGGGTGGCTGTTCT-3′
Zbtb46	5′-CAGAGAAGAACTGCTGTGTACGG-3′	5′-CAGACAGAAGTTGGCATGGTAGC-3′
Bmi	5′-CATTGGGCCATAGTTTGTTAATCTCAA-3′	5′-CCAATATGGCATTGTACAACAAGC-3′
Hes5	5′-TCACCAGGGCCGCCAGAGGCCG-3′	5′-ATGGCCCCAAGTACCGTGGCGG-3′
STMN	5′-CCAGAATTCCCCCTTTCCCC-3′	5′-CCAGCTCTTCAAGACCTCA-3′
TGFβ	5′-CAGAGAAGAACTGCTGTGTACGG -3′	5′-CAGACAGAAGTTGGCATGGTAGC-3′
GAPDH	5′-GTATGTCGTGGAGTCTACAG-3′	5′-GAGTTGTCATATTTCTCGTGGT-3′

Supplemental data 1 Differential gene expression between primary NSCs and astrocytes.

Supplemental data 2 Differential gene expression between primary NSCs and induced astrocytes (Oct4 for 5 d)

Supplemental data 3 Differential gene expression between primary NSCs and induced astrocytes (Oct4 for 7 d)

Supplemental data 4 Differential gene expression between primary NSCs and induced astrocytes (Oct4/Shh for 5 d)

Supplemental data 5 Differential gene expression between primary NSCs and induced astrocytes (Oct4/Shh for 7 d)

2. Supplemental Experimental materials and Procedures

Main reagents

Dulbecco's modified Eagle's medium (DMEM) with high glucose (6 g/L), DMEM/F12, normal donkey serum, fetal calf serum (FCS), G5 supplement, TRIzol,

and trypsin were purchased from Invitrogen (USA); poly-L-lysine (PLL), 3-(4,5)-dimethylthiazol-2-yl)-2,5-diphenyltetrazolium bromide (MTT), HEPES, ethylenediamine tetraacetic acid (EDTA), bovine serum albumin (BSA), retinoic acid (RA), nerve growth factor (NGF), brain-derived neurotrophic factor (BDNF), bromodeoxyuridine (BrdU), penicillin, streptomycin, RA, and D-Hanks were purchased from Sigma-Aldrich (USA); a Shh peptide was purchased from R&D (USA); NU9516 was purchased from MCE (USA); GDC-0941 was purchased from Selleck(China); USF2 was purchased from Origene (USA); anti-nestin antibody, anti-glial fibrillary acidic protein (GFAP) antibody, anti-Pax6 antibody, anti-CD133 antibody, anti-SYN antibody, anti-GABA antibody, anti-PSD-95 antibody, anti-vGluT1 antibody, anti-Oct4 antibody, anti-GLT1 antibody and horseradish-conjugated secondary antibody were obtained from Abcam (USA); anti-NeuN antibody was purchased from(Merck); anti-Tuj-1 antibody, anti-CNP antibody, anti-actin antibody, and rabbit anti-BrdU antibody were purchased from Millipore (USA); anti-Nolz1 polyclonal antibody was purchased from Biocompare (USA); anti-Ptch antibody, anti-Gli2 antibody anti-cyclinD1 antibody, anti-vGluT1 antibody, anti-MAP2 antibody, anti-Smurf2 antibody, anti-CDk2 antibody, anti-Nozl antibody, anti-PI3K antibody, anti-Sox2 antibody, anti-Homer1 antibody, and anti-pPI3K antibody were purchased from CST (USA) and a 4',6-diamidino-2-phenylindole (DAPI) staining kit, Alexa Fluor 488-conjugated donkey anti-mouse IgG, CMFDA, and Alexa Fluor 594-conjugated goat anti-rabbit antibody were purchased from Molecular Probes (USA). An RNA isolation kit was obtained from Promega (USA). A bicinchoninic acid (BCA) kit and RNeasy Mini Kit were purchased from Qiagen (Germany). An RT-PCR kit was purchased from Takara (Japan).

Production of Oct4 recombinant Lentivirus

To produce lentiviral particles, rat Oct4 cDNA was first amplified using a high-fidelity DNA polymerase and subsequently cloned into a pGMLV-based lentiviral vector as previously described by Xu et al [58]. The Oct4 primer sequences for RT-PCR are shown in Table S1. After verifying correctness of constructed vectors,

pGMLV lentiviral vectors containing Oct4 cDNA were transfected into 293T cells using Lipofectamine 2000 transfection reagent to package the Oct4 pseudotyped virus. The virus-containing supernatant was collected after 36 to 48 h of transfection, filtered through a 0.45 μm syringe filter, and further concentrated by ultracentrifugation to establish virus stocks. Subsequently, the virus stocking solution was aliquoted 50 μl per tube and stored at −80 °C for the subsequent experiments.